

Accepted manuscript doi: 10.1680/jgeot.18.P.311

Accepted manuscript

As a service to our authors and readers, we are putting peer-reviewed accepted manuscripts (AM) online, in the Ahead of Print section of each journal web page, shortly after acceptance.

Disclaimer

The AM is yet to be copyedited and formatted in journal house style but can still be read and referenced by quoting its unique reference number, the digital object identifier (DOI). Once the AM has been typeset, an 'uncorrected proof' PDF will replace the 'accepted manuscript' PDF. These formatted articles may still be corrected by the authors. During the Production process, errors may be discovered which could affect the content, and all legal disclaimers that apply to the journal relate to these versions also.

Version of record

The final edited article will be published in PDF and HTML and will contain all author corrections and is considered the version of record. Authors wishing to reference an article published Ahead of Print should quote its DOI. When an issue becomes available, queuing Ahead of Print articles will move to that issue's Table of Contents. When the article is published in a journal issue, the full reference should be cited in addition to the DOI.

Accepted manuscript doi: 10.1680/jgeot.18.P.311

Submitted: 19 November 2018

Published online in ‘accepted manuscript’ format: 15 September 2020

Manuscript title: Physical modelling to demonstrate the feasibility of screw piles for offshore jacket supported wind energy structures

Authors: Craig Davidson*, Michael John Brown*, Benjamin Cerfontaine*, Therar Al-Baghdadi[†], Jonathan Knappett*, Andrew Brennan*, Charles Augarde[‡], William Coombs[‡], Lei Wang[‡], Anthony Blake[§], David Richards[§] and Jonathan David Ball^l

Affiliations: *School of Science and Engineering, University of Dundee, Fulton Building, Dundee, UK; [†]Municipality of Karbala, Karbala, Iraq; [‡]Department of Engineering, Durham University, Durham, UK; [§]Faculty of Engineering and the Environment, University of Southampton, UK and ^lRoger Bullivant Ltd, Burton Upon Trent, UK

Corresponding author: Craig Davidson, School of Science and Engineering, University of Dundee, Fulton Building, Dundee, DD1 4HN, UK.

E-mail: c.s.davidson@dundee.ac.uk

Abstract

Screw piles potentially offer quieter installation and enhanced axial tensile capacity over straight-shafted driven piles. As such, they have been suggested as a possible foundation solution for offshore jacket supported wind turbines in deeper water. To investigate the feasibility of their use in this setting, centrifuge testing of six model screw piles of different designs was conducted to measure the installation requirements and ultimate axial capacity of the piles in very-dense and medium-dense sand. The screw piles were designed to sustain loads generated by an extreme design scenario using published axial capacity and torque prediction formulae. Single and double-helix designs, including an optimised design, intended to minimise installation requirements, with reduced geometry were installed and tested in-flight. Piles in the medium-dense sand for example had significant installation requirements of up to 18.4MNm (torque) and 28.8MN (vertical force) which were accurately predicted using correlations with cone resistance data (CPT). Existing axial capacity design methods did not perform well for these large-scale screw piles, overestimating compressive and tensile capacities. Revised analytical methods for installation and axial capacity estimates are proposed here based on the centrifuge test results.

Keywords: Offshore engineering; Piles & piling; Torsion

Introduction

Currently, 81% of existing offshore turbines in Europe are supported by monopile foundations, with gravity base structures and jackets making up the remainder (Windeurope Business Intelligence, 2017). Monopile foundation diameters have increased from typically 4m (LeBlanc et al., 2010), suited to water depths up to 25m (DNV, 2010), to 7.8m diameter in 41m water depth at the Veja Mate wind farm (EEZ2 German North Sea). Monopiles with diameters of 10m or more are expected in forthcoming developments (Byrne et al., 2017) and although these can be manufactured, their installation may prove challenging. Others argue that monopiles have already reached their practical maximum or economically viable size (Golightly, 2014) at 10m in diameter in 45m water depths and that investment should be placed in developing more cost effective alternatives.

As wind energy moves into deeper water (>45m), piled steel jackets may become the preferred solution. For example, the Beatrice Wind Farm (Moray Firth, UK) uses jackets situated in up to 55m water depth with single tubular piles (2.2m diameter and 35 – 60m long) driven at each corner (Beatrice Offshore Windfarm Ltd, 2017). With increasing water depth, it may be necessary to increase the numbers of piles per jacket. Consequentially, for a wind farm with maybe hundreds of turbines, at least 3 to 4 times as many (and possibly many more) piles would need to be deployed for jacket structures. This would result in long duration pile driving operations raising concerns over the effects of noise and vibration on marine inhabitants (JNCC, 2010). Such concerns have led to tight controls on offshore pile driving (Huisman, 2019) such as maximum times to drive piles and limits on underwater noise during driving and/or the need to implement expensive noise mitigation measures (Bruns et al., 2014).

With these challenges facing jacket deployment, alternative foundation types are being explored. One onshore technique with potential is screw piles. Currently this type of steel pile has a low diameter tubular core (typically 64 – 200mm) with one or more (average of 2 (Perko, 2009)) larger diameter (typically 150 – 400mm) helical plates (helices) welded to the central core (Perko, 2009, Sakr, 2015), as shown in Figure 1. They are commonly installed onshore by a 360° excavator using a hydraulic torque head that rotates the pile, while vertical or “crowd” force is applied by the boom/arm of the excavator (Perko, 2009) as required. This type of pile, known for their high tensile capacity and quick installation with low noise and vibration, is attractive for potential use with jackets for offshore wind, but also as a potential anchor for future floating wind or wave energy converters (Byrne and Houlby, 2015).

The combined axial and lateral loads in the offshore environment present a particular difficulty in developing screw piles for the offshore wind sector. Most onshore screw pile applications are subject to relatively low lateral loads resulting in the pile geometry in Figure 1, with typical helix diameter (D_h) to core diameter (D_c) ratios (D_h/D_c) of 1.5 to 8 (average 3.3) (Perko, 2009, Sakr, 2015). Therefore, for offshore deployment it is envisaged that the pile geometry will need to change significantly (Al-Baghdadi et al., 2017a) with a particular need to increase the structural bending moment capacity (Al-Baghdadi et al., 2015) through an increased core diameter or upper section.

Previous screw pile studies in sand (Knappett et al., 2014, Al-Baghdadi, 2018) indicate that greater efficiencies can be achieved under vertical compressive loading by varying the helix to core diameter ratio (D_h/D_c) and in the case of multi-helix designs, changing the vertical spacing of the helices (S/D_h). Such variations in geometry and diameters are well outside the current experience of onshore screw pile design (Perko, 2009, Das and Shukla, 2013, BS 8004:2015) and deployment. This is of particular concern when adopting screw piles for offshore wind applications where it is likely that new plant will be needed to accommodate

the large installation loads and torque. In turn, this means that the geometries required offshore may not be controlled only by in-service or extreme loading but may need to be optimised to reduce installation requirements (Morais and Tsuha, 2014). Current prediction of installation torque is based upon: correlation of field measured torque with anticipated or measured pile capacity (Hoyt and Clemence, 1989, Perko, 2009); modification of empirical pile capacity design methods (Ghaly and Hanna, 1991, Tsuha and Aoki, 2010, Sakr, 2015); or is related to in situ testing such as Cone Penetration Testing (CPT) (Gavin et al., 2013, Spagnoli, 2016, Al-Baghdadi et al., 2017b, Davidson et al., 2018a) for much smaller piles. These methods show wide scatter in predicted torque values and/or may have seen limited validation for a limited range of pile sizes and configurations.

The design case considered in this paper, consists of an 8MW turbine on a four-legged steel jacket in 80m water depth, founded on a single screw pile at each corner, in either medium-dense or very-dense sand. This scenario allows quantification of upper-bound installation and in-service loads that may be placed upon an appropriately modified pile geometry. Six screw pile designs, theoretically capable of sustaining loads from this design scenario were fabricated at model scale and tested to determine their installation requirements and axial capacities. Of the six piles, four were designed for the very-dense sand condition based on existing methods (e.g. Mitsch and Clemence (1985) and Perko (2009)), while the design of a further two piles for the medium-dense sand state were based upon modifications to the existing design methods, which are discussed in this paper, following the test results of the first four screw piles. An analysis of these design methods is performed and recommendations given to new design approaches based on centrifuge modelling, as well as to the feasibility of using large screw piles as offshore wind turbine jacket structure foundations

Methodology

Assessment of Loads: Design scenarios

Jackets to support offshore wind turbines are likely to be deployed in water depths of 45 to 80m, between the proven capability of monopiles and potential future floating structures. Therefore, the worst-case design scenario was to select the deepest water conditions coupled with a suitably large wind turbine of 8MW size. A homogenous sand profile consisting of either medium-dense ($D_r = 57\%$) or very-dense ($D_r = 84\%$) sand was considered to investigate the relationships between pile geometry, installation requirements and axial capacities generated from the differing soil properties.

The jacket and turbine used in the scenarios are shown in Figure 2. The vertical force transmitted from the jacket to the foundation comprises the self-weight of the steel (density of 7800kg/m^3), ancillary equipment weighing 2MN and heavy marine growth as per DNV (2007). The dead load of the wind turbine was derived from the Leanwind (2013) 8MW turbine. Parameters representing environmental conditions with a 1% exceedance level in the North Sea (Table 1) were used to determine the wind and wave loads using DNV (2007). The wind speed adopted was above the operational limit of the turbine and therefore the blades were assumed to be statically positioned as in Figure 2, at an angle of attack to present the largest surface area possible to the wind.

All loads were assumed to act in unison, diagonally across the jacket to calculate the upwind tensile and downwind compressive loads. A pinned jacket-foundation pile connection was assumed, and calculations were undertaken using a factor of 1.35 on the final loads for each pile (a value provided confidentially by an offshore consultant undertaking this type of design on a commercial basis). This resulted in each pile requiring capacities of 3.08MN laterally, 32.31MN in compression and 24.23MN in tension.

Screw pile design process

Initially, it was envisaged that multi-helix screw piles with helix spacing (S) equal to $2 - 3D_h$ would be the most appropriate design solution over a single-helix approach, due to the expected enhanced compressive axial capacity, as suggested by Knappett et al. (2014) and Al-Baghdadi (2018). Therefore, multi-helix piles were designed, with single-helix designs considered for comparison. Initially, only the very-dense sand scenario was investigated in the physical model testing to prevent unnecessary remanufacturing of model screw piles for subsequent tests if the results were unfavourable. The process for the multi-helix screw piles in the very-dense sand followed the steps outlined below to calculate the various components contributing to the relevant capacity.

Following analysis of the tests results from the very-dense sand scenario, with respect to the measured versus predicted values for installation and axial loads, the medium-dense sand scenario piles were designed. This process used a modified procedure from that used in the very-dense sand scenario and is described in the Results section of the paper (Methods 1c and 3t).

Step 1: Lateral capacity and initial assumptions

The shaft or core diameter, wall thickness (t_s) and material properties of the core were established through analytical lateral and moment capacity methods, outlined in Randolph and Gourvenec (2011), to determine the lateral load capacity of the screw pile (acting as a conventional pile). The axial capacity of a screw pile with multiple helices spaced at $2D_h$ apart act in a cylindrical-shear arrangement. The adopted design approaches varied with tensile or compressive conditions as described below.

Step 2: Tensile Axial Capacity (Method 1t)

The tensile capacity calculation followed the method developed by Mitsch and Clemence (1985) and prescribed by Das and Shukla (2013) and is equal to the sum of Equations (1) and (4). The tensile cylindrical shear resistance (Q_{st}) generated along the soil-soil shear interface between the helices at their perimeter is determined by Equation (1), where the peak friction angle (ϕ'_{pk}) is used and K_u is the earth pressure coefficient of a screw pile in uplift as determined by Mitsch and Clemence (1985). K_u is calculated in Equation (2), where m defines the gradient of the linear relationship between K_u and the ratio of the depth (H) to diameter (D_h) of the helix of interest (H/D_h) as a function of the peak soil friction angle. The values of m , presented in Table 2, were derived by Mitsch and Clemence (1985) from their uplift capacity tests of helical anchors in sand. The length of the cylinder is determined by the depth of deepest helix (H_1) minus the depth of the shallowest helix (H_n). The diameter of the shallowest helix is denoted as D_{hn} and when helices of different diameter are specified the average diameter (D_{ha}) is used.

$$Q_{st} = \sigma'_v K_u \tan \phi'_{pk} \pi D_{ha} (H_1 - H_n) \quad (1)$$

$$K_u = 0.6 + m \frac{H_n}{D_{ha}} \quad (2)$$

The helix tensile capacity (Q_{ht}) generated by the uppermost helix can have either a shallow or deep failure mechanism depending on the embedment depth of the helix. A shallow failure mechanism results in a conical failure surface, emanating from the shallowest helix, reaching the soil surface (Figure 1) (Cerfontaine et al., 2019a), whereas a flow-around mechanism occurs for deeply embedded helices and the failure plane terminates below the surface instead. The initial approach adopted was to design the screw piles to operate with a shallow

failure mechanism in uplift. The formation of the soil wedge from the uppermost helix to the soil surface obscures the limited contribution from shear-resistance along the soil-steel interface of the shaft and thus the shaft resistance is not included in the tensile capacity, in line with Ghaly et al., (1991) and also as demonstrated by Cerfontaine et al., (2019a) from finite element modelling. In the case of a shallow failure mechanism, the non-dimensional breakout factor (F_q), which is dependent on the soil friction angle can be calculated from Equation (3) as shown in Figure 3, with the ultimate uplift capacity (Q_{ht}) of the helical plate calculated by Equation (4). The earth pressure coefficient and thus the breakout factor reach a maximum value when the failure mode transitions to a deep mechanism, at an embedment ratio which is dependent on the soil friction angle, as defined by Mitsch and Clemence (1985). Horizontal lines in Figure 3 show the ultimate values of the breakout factor for deep failure conditions.

$$F_q = \left(\frac{H_n}{D_{hn}}\right)^2 K_u \tan \phi'_{pk} \cos^2 \frac{\phi'_{pk}}{2} \left(0.5 \frac{H_n}{D_{hn}} + \frac{1}{3} \tan \frac{\phi'_{pk}}{2}\right) + 1 + \frac{1}{3} \left(\frac{H}{D_{hn}}\right)^2 \tan^2 \frac{\phi'_{pk}}{2} \quad (3)$$

$$+ 2 \left(\frac{H}{D_{hn}}\right)^2 \tan \frac{\phi'_{pk}}{2}$$

$$Q_{ht} = F_q \sigma'_v A_h \quad (4)$$

Step 3: Compressive Axial Capacity (Method 1c)

The compressive capacity predictions of the proposed screw piles were calculated from the sum of the shaft and cylindrical-shear resistances (cylindrical-shear mechanism) (Figure 1) and the bearing resistance of the bottom helix and pile tip using Equations (6) to (8). Values of the lateral earth pressure coefficient (K_{uc}) were determined from the values recommended by Mitsch and Clemence (1985) and represented as an equation by Perko (2009) as shown in Equation (5). The compressive cylindrical shear capacity was then calculated using Equation (6).

$$K_{uc} = 0.09 e^{0.08 \phi'_{pk}} \quad (5)$$

$$Q_{sc} = \sigma'_v K_{uc} \tan \phi' \pi D_h (H_1 - H_n) \quad (6)$$

The shaft resistance contribution to the compressive capacity was calculated with Equation (7) and as suggested by Zhang (1999), Tappenden and Segio (2007), Elsherbiny and El Naggari (2013), Mohajerani et al. (2016), a portion of the shaft, equal to one helix diameter, above the upper helix does not contribute to the shaft capacity. This is at odds with Perko (2009) who recommends that the soil-steel component of the shaft capacity of small diameter piles is conservatively neglected due to installation disturbance but he does suggest that larger diameter shafts may derive some of their capacity from shaft resistance.

$$Q_s = \sigma'_v K_{uc} \tan \delta'_{crit} \pi D_c (H_n - D_{hn}) \quad (7)$$

Following standard foundation capacity calculations, a bearing capacity factor (N_q) was used to determine the compressive capacity (Equation (8)) of the lowermost helix (Q_{hc}). In this calculation, the full area of the helix was used, based on the assumption that the open-ended pile shaft would either plug during installation or behave in a plugged manner under compressive loading (Randolph and Gourvenec, 2011). Meyerhof (1951) bearing capacity factors (Equation (9)) were used in an unrestricted manner, i.e. the values were not limited with depth as is proposed in some approaches.

$$Q_{Hc} = N_q A_h \sigma'_v \quad (8)$$

$$N_q = e^{\pi \tan \phi'_{pk}} \tan^2 \left(45 + \frac{\phi'_{pk}}{2} \right) \quad (9)$$

Step 4: Installation Torque

The helix pitch and plate thickness were selected with values chosen to be consistent with those used by Al-Baghdadi (2018) in previous centrifuge modelling of screw piles in sand and with those reported in Spagnoli and Gavin (2015).

To determine a suitable installation torque prediction method, existing analytical (Ghaly and Hanna, 1991, Sakr, 2015) and CPT methods (Gavin et al., 2013, Spagnoli, 2016, Al-Baghdadi et al., 2017b) were compared for the single-helix pile reported in Al-Baghdadi et al. (2017b). As a full suite of CPT cone resistance data (q_c) data was unavailable for the CPT torque correlations, synthetic q_c data was calculated based on relative densities of 31, 55 and 73% using the method of Baldi et al. (1986). The resulting torque predictions are shown in Figure 4, showing significant differences between the methods. As a result, the analytical methods were discounted in the design process and the Al-Baghdadi et al. (2017b) method (Appendix A) was selected, as analysis by Al-Baghdadi (2018) suggested a good correlation for multi-helix screw piles, while both Gavin et al. (2013) and Spagnoli (2016) present verification of their methods on single-helix screw piles only.

The predicted installation torque was checked against the torsional capacity (T_{max}) (Equation (10)) of the screw pile shaft to ensure that structural failure would not occur during installation.

$$T_{max} = \frac{\pi}{16} \tau_{steel} \frac{(D_c^4 - (D_c - 2t_s)^4)}{D_c} \quad (10)$$

where τ_{steel} is the shear strength of the steel in the pile shaft.

Screw pile designs

The naming system for the screw pile designs tested in this paper has an initial letter which denotes the use of optimisation in the design (U = uniform; O = optimised i.e. a stepped diameter to provide greater lateral resistance through a large diameter near-surface whilst reducing installation torque through smaller diameter at depth (Davidson et al., 2018b)). The following number denotes the number of helices while the next two letters describe the soil density (VD = very dense, MD = medium dense). The final letter denotes differences

between similar designs for the same scenario. Model and prototype dimensions of the screw piles in Figure 5 are presented in Table 3.

The first screw pile design (U2VD) for the very-dense sand scenario is presented in Figure 5a. During the design process, the tensile capacity was found to be the most critical design step, with relatively deep embedment of the uppermost helix required to meet the design loads. Placing the upper helix at a greater depth while maintaining $S/D_h = 2$ resulted in the compressive capacity being significantly over-rated with respect to the design load as N_q increased with depth.

The requirement to place the upper helix at a relatively deep embedment necessarily required significant shaft length. Al-Baghdadi (2018) demonstrated that the shaft contributed the greatest amount to the total installation torque. Therefore, an investigation was conducted to optimise the screw pile geometry where possible to reduce the torque. From the calculations of the lateral capacity, it was found that the screw pile shaft would be expected to fail in a 'long-pile' failure mode where a plastic hinge is assumed to form in the pile at some depth (Randolph and Gourvenec, 2011). Therefore, $1.24D_c$ below the depth of the predicted plastic hinge point, the shaft diameter was reduced. Furthermore, as the compressive capacity was greater than required, the lower helix diameter was also reduced to a diameter which gave a predicted capacity closer to the design load. Torsional capacity checks were again performed and the design iteratively refined until all capacities were satisfied, resulting in the design (O2VD) shown in Figure 5b which had a 67% reduction in predicted torque (using the method in Al-Baghdadi et al. (2017b)) over the non-optimised design in Figure 5a.

To provide a benchmark against which the double-helix designs could be compared, the single-helix design (U1VD-A) in Figure 5c was also created by following the steps previously outlined. Although the predicted capacities of this design satisfied the design requirements, a further single-helix screw pile (U1VD-B) was created based upon the non-optimised (U2VD) design, by removing the upper helix, to investigate the effectiveness of the cylindrical shear component of the U2VD design and of increasing H/D_h in the U1VD-A single helix design. The embedment ratios (Table 3) for the shallowest helix of these screw piles are less than the values presented by Mitsch and Clemence (1985) for the transition from shallow to deep failure mechanisms and therefore a shallow failure mechanism should be expected for all designs presented.

Centrifuge Testing

To replicate prototype stress conditions, geotechnical centrifuge testing of scaled model piles was conducted. The model piles had solid cores to avoid structural failure and scaling issues with testing open-ended piles where plugging may occur prematurely due to grain size effects. Thus, the fully plugged pile behaviour resulted in upper bound measurements of installation loads.

Pile testing was undertaken on the University of Dundee 3m radius geotechnical centrifuge at 48g in a box with internal dimensions of 500 x 800 x 550mm using a dedicated screw pile actuator developed to allow installation and testing of a single pile in one operation (inflight) (Al-Baghdadi et al., 2016). Two tests were undertaken in each box with manual repositioning of the actuator between flights and considering the box as effectively split into two halves to maximise results. Axial loads and torque were measured during installation and subsequent load testing using a combined torque-load cell (Novatech Measurements Ltd F310-Z, 20kN/30Nm capacity), while displacement was measured with a draw-wire sensor (Davidson et al., 2018b). Tests in dry sand at 48g result in in situ effective stresses equivalent to saturated sand at 80g due to the increased dry unit weight (Li et al., 2010). On this basis, the tests and piles were actually scaled at 1:80 from the prototype case.

Sand beds, pluviated to a depth of 430mm at average relative densities of $D_r = 84\%$ and $D_r = 57\%$ for the very-dense and medium-dense scenarios respectively, used HST95 sand which is a fine-grained quartz sand (Table 4). For the $D_r = 84\%$ sand tests, the shortest distance to the container boundaries from the test locations was greater than $7D_h$ (Phillips and Valsangkar, 1987, Bolton et al., 1999). However, actual radial interference for a screw pile during installation is likely to be associated with volume change from the pile core rather than the helix, resulting in $14D_c$ minimum separation from the side boundaries. The minimum spacing to the side wall was greater than $3D_h$ or $10D_c$ in the $D_r = 57\%$ sand. The smallest pile shaft diameter gave a minimum value of $53D_{50}$ satisfying the recommendations by Garnier et al. (2007) regarding the ratio of pile to average grain size diameters. Similarly, the ratio of the smallest helix diameter to average grain size is equal to 120, which is greater than the minimum of 58 proposed by Schiavon et al. (2016).

The piles were installed using displacement control to advance vertically by an amount equal to the helix pitch per revolution (Perko, 2009) (i.e. at 7mm per revolution at 3RPM) sometimes referred to as “pitch matched” or “perfect” installation (Lutenegger, 2019). Pitch matched installation is generally recommended to minimise soil disturbance and improve in-service pile performance (Perko, (2009) and BS 8004:2015, (2015)). Tensile and compression load tests were undertaken at 1mm/min up to a typical displacement of 10mm ($0.4 - 0.6D_h$) at model scale. Torque and vertical force values for the full centrifuge test duration, from spinning up the centrifuge to the operating g-level (stage 1), through installation (stage 2) to the end of the axial capacity test (stage 3) are shown in prototype scale units for pile U1VD-B in Figure 6, for both compression and tensile tests. Intervals between the described stages represent monitoring periods. All data are offset by the respective values recorded immediately before the installation phase of the test. This results in a non-zero value at the start of the test sequence in Figure 6. The testing programme is summarised in Table 5 for the 12 tests conducted.

Cone Penetration Tests (CPT)

Cone penetration tests (CPT) were conducted in sand of $D_r = 52$ and 82% at 20mm/min rate of penetration using an Actidyn In-Flight Loading System (P67-2L) and Actidyn CPT probe of 12mm diameter, giving a $B/D_{50} = 86$ which exceeds the limiting B/D_{50} ratio of 20 suggested by Bolton et al. (1999). The resulting q_c data from the tests are shown at prototype scale in Figure 7.

Results and discussion

Installation Torque

Measured torque from all tests with “perfect” installation are shown at prototype scale in Figure 8. The 5.97 to 7.49MNm required to install the optimised and uniform screw piles respectively in very-dense sand is substantial, although equipment such as casing rotators can provide up to 7.4MNm of torque and may be suitable in terms of the installation torque required for very-dense sand (particularly for the optimised designs).

Comparing the performance of the optimised and non-optimised piles (U2VD and O2VD respectively) in Figure 8 shows there is potential to reduce the torque requirements through geometry optimisation. The 11% reduction in the screw pile surface area of the optimised design produced a 17% reduction in torque; comparable to the 33% drop found by Morais and Tsuha (2014) for a 28% reduction in screw pile surface area of field tested smaller onshore piles. Any further reduction in pile geometry was not possible in this study without compromising the structural integrity of the screw pile.

The decreased soil strength associated with the reduction in relative density from $D_r = 84$ to 57% is not sufficient to offset the greater torque generated by the larger screw pile geometry required to provide sufficient axial capacity in the medium-dense sand. Thus, the 10.18MNm (U1MD) to 18.37MNm (U2MD) (Figure 8) measured in the medium-dense screw pile tests would appear to be beyond the capacity of any existing equipment and would require the development of new equipment for installation.

Both of the single helix piles (U1VD-A and U1VD-B) in the very dense sand tended to the same final torque as the optimised double helix pile (O2VD) with the effect of optimised shaft diameter from pile O2VD only being apparent up to a depth of 9.8m in Figure 8. The effect of the second helix on the torque became apparent at approximately 6m depth, where the torque values of the single-helix (U1VD) and double-helix (U2VD) diverged as the second helix began to engage with the sand. The single and double-helix very-dense sand designs differed by 1.39MNm at 12.9m, indicating the additional torque required to install the second helix.

The torque measured during installation of all screw piles was higher than the anticipated values from the Al-Baghdadi et al. (2017b) prediction method (e.g. Figure 9 for piles U2VD, U1VD-B, O2VD and U1MD), which was developed alongside an installation force prediction method in Appendix C (Al-Baghdadi et al., 2018) from centrifuge tests of screw piles with various geometries in dense and medium-dense sand. Figure 9 also shows an updated version of the Al-Baghdadi et al. (2017b) method proposed by Davidson et al. (2018a) and summarized in Appendix B. The Davidson et al. (2018a) equations modified the previous Al-Baghdadi et al. (2017b) correlations in several ways: by omitting the rotation force reduction factors proposed for the shaft and base components as they are larger than that suggested by Deeks (2008) and their use is not clearly defined; the full cone resistance (q_c) value is employed instead of $0.6q_c$; a missing $\tan(\delta_{crit})$ term was added to base component; and the stress drop index (a) is related to the CPT friction ratio and interface friction angle instead of $a = 0.03$. In addition to these methods, predictions are also shown using Ghaly and Hanna (1991), Gavin et al. (2013), Sakr (2015), and Spagnoli (2016) methods. The analytical methods of Ghaly and Hanna (1991), and Sakr (2015) both over-predict the required installation torque (by up to 53% and 84% respectively in the tensile test of pile U2VD). Sakr (2015) reported an increased accuracy over Ghaly and Hanna (1991) as effective stress was incorporated instead of total stress. For double-helix designs, the effective stress on the lower helix calculated in the Sakr (2015) formulae is based on the package of soil between the helices and is thus limited in magnitude. Unlike Ghaly and Hanna (1991) who proposed a 70% reduction of the lateral earth pressure (K_p) for the torque acting on the shaft, Sakr (2015) employs the full value of K_p .

The Gavin et al. (2013) and Spagnoli (2016) CPT-torque prediction methods were conceived for single helix screw pile designs, but the addition of further helices is considered possible by repeating the helix torque calculations for the additional helices (at their respective depths) using the appropriate formulae from each method. These additional calculations were performed for the double-helix designs (U2VD, O2VD and U2MD) to investigate the effectiveness of the Gavin et al. (2013) and Spagnoli (2016) CPT-torque correlations on multi-helix screw pile designs. Analysis of the CPT-torque prediction methods by Gavin et al. (2013) and Spagnoli (2016) in Figure 9 indicates generally good predictions for the non-optimised (U1VD-B) single helix pile for which these methods were derived in dense sand. Unfortunately, though when the methods are applied for a single helix pile in medium dense sand both methods significantly overpredict torque (166% and 164% for Gavin et al. (2013) and Spagnoli (2016) respectively) and appear sensitive to changes in the data that are not

apparent in the other prediction techniques. It is interesting to note though that in the case of U2VD that the Spagnoli (2016) method again appears to work well for additional helices as does the Gavin et al. (2013) method up to a depth of approximately 6.2m. Below 6.2m the Gavin et al. (2013) method begins to overpredict the installation torque. This depth coincides with an increase in the CPT cone resistance, relating to a minor change of 2-3% relative density, (Figure 7) and highlights the sensitivity of the predicted torque values to the raw q_c values used in the Gavin et al. (2013) method compared to the methods which use averaged q_c data (Spagnoli (2016), Al-Baghdadi et al (2017b) and Davidson et al (2018)).

Installation Force

To date, concern over offshore deployment of screw piles has centred around predicting torque (Byrne and Houlsby, 2015). However, the prototype vertical forces measured during the installation of the pitch matched (or “perfect” installation) screw piles herein have considerable magnitudes which would pose significant challenges to the use of screw piles offshore. The final installation compressive forces of the designs tested range from 13.3 to 28.8MN (Figure 10). The self-weight of the casing-rotators previously discussed are less than 1MN and would thus require significant reaction to enable their use. In onshore screw pile installation, vertical or “crowd” forces are rarely measured, although for quality control and torque prediction this along with rates of installation should become routine. This lack of consideration of installation force is reflected in the literature with only two prediction methods currently available. Ghaly and Hanna (1991) analytically consider the vertical forces acting on the shaft and the upper and lower surfaces of the helices under total stress conditions while Al-Baghdadi (2018) correlates installation force with q_c via Equations C1 – C7 in Appendix C.

Predictions of the installation force for pitch matched installation using both methods for all piles are given in Figure 11a – d. In all tests, the prediction using Equations C1 – C7 in Appendix C provide a close match with the measured force, whereas the Ghaly and Hanna (1991) equations only appear to work for the final value in the $D_r = 84\%$ tests of piles U1VD and U2VD. In the $D_r = 57\%$ tests, the Ghaly and Hanna (1991) method over-predicts below a depth of approximately 7.5m, indicating that the second helix does not affect the outcome of the prediction method and that the formulae are not applicable to medium-dense sand. Al-Baghdadi (2018) proposed that the rotation reduction factor, f , in Equation C2 and C3 are related to the relative density, but a constant value of $f = 0.6$ was more appropriate for the tests herein and is similar to that found by Deeks (2008), Garcia-Galindo (2017) and Garcia-Galindo et al. (2018).

Comparing the results in Figure 11b and c shows that optimizing the screw pile geometry can reduce the installation force, where a reduction of the volume of steel in the shaft of 18% resulted in a 34% reduction in force. Linking this drop in force to the reduced core volume as per Al-Baghdadi (2018), is further verified by the similarity in force between the non-optimised single (U1VD-B) and double-helix (U2VD) piles where the addition of another helix has a relatively limited effect on the installation force.

Compressive Capacity Tests

The centrifuge installation rig used separate motors to control the rotary and vertical motion (Al-Baghdadi et al., 2016). These motors were synchronised to operate together which leaves a residual force on the pile at the end of the installation, which is clearly visible at the end of stage 2 in Figure 6a and b. This residual force is evident at zero displacement in the results of compression testing in Figure 12a, where the data starts from a non-zero value on the y-axis of the measured compressive capacity (Q_{cm}). However, this is not considered to affect the

ultimate capacity, which is taken as the measured force (Q_{cm}) at a displacement (z) of $0.1D_{ha}$ (Al-Baghdadi, 2018) (Table 6).

Considering the measured capacity of each pile in relation to the required compressive capacity of 32.31MN from the design scenario; designs U2VD, U1MD and U2MD exceed the requirements, while the remaining piles (U1VD-A, U1VD-B and O2VD) do not, as shown in Table 6. The results for the optimised pile (O2VD) are somewhat disappointing in that this pile was designed to reduce installation requirements whilst maintaining sufficient compressive capacity. However, although the compressive capacity is 39.5% lower than the non-optimised (U2VD) pile, it is also 34.5% below the required compressive capacity from the prescribed design scenario.

The empirical relationship proposed by Hoyt and Clemence (1989) and widely adopted by the screw pile industry, provides a parameter, K_t , which relates the axial capacity to the final installation torque value (Equation (11)). This correlation suggests that the capacity of a given shaft diameter should be unique at a specific installation torque and therefore, the capacity of the optimised pile (O2VD) should be lower than the non-optimised version (U2VD) since they have different shaft diameters. However, this relationship is not considered an appropriate way to calculate the capacity of a screw pile. From the results of numerous field tests presented in Perko (2009), significant scatter is apparent in the data, which draws into question the supposed uniqueness of this relationship, although this may also reflect the of the potential for a lack of installation control in the field. From this data, Perko (2009) suggests a method to calculate K_t for a given shaft diameter in Equation (12).

$$Q = TK_t \quad (11)$$

$$K_t = \frac{1433}{D_c^{0.92}} \quad (12)$$

Using Equation (12), values of K_t were calculated using the minimum shaft diameter for the reported screw pile designs and compared to the K_t values calculated from Equation (11) using the measured capacity and installation torque (Table 7). Differences of up to 283% between the theoretical and back-calculated values of K_t were observed. Using the theoretical K_t values for these designs would lead to significant over-estimations of the tensile capacity. Furthermore, Perko (2009) states that it is permissible to use the same value of K_t for both compression and tension. Table 7 highlights that this would also be inappropriate for the large screw piles presented, with significant differences observed between the back-calculated values of K_t for tensile and compressive conditions. This suggests that for the piles investigated here that capacity determination based upon torque measured during installation is inappropriate as would be inferring torque requirements from capacity calculations. Lutenegger (2019) highlights that correlations of torque to capacity are often assumed to be the same whether one or two helices are included (i.e. the inclusion of additional helix plates is ignored) and goes on to show that the torque encountered during installation is also affected by the pitch of a helix plate, while the capacity is unaffected. Thus, non-unique values of K_t can be observed for screw piles with the same shaft diameter. The values of K_t in Table 7 from the centrifuge tests confirm that non-unique values of K_t are observed between piles with the same shaft diameter, but different numbers of helices in the same relative density. The observed K_t values also appear to decrease with shaft diameter, in line with previous observations on smaller diameter piles (e.g. Perko, (2009)).

It is noted that both of the single-helix very-dense piles (U1VD-A and U1VD-B) have a slightly greater compressive capacity than the optimised double-helix pile and therefore the only slight advantage of the optimised double-helix design over the single-helix piles is a reduced installation force and slightly less energy required to overcome the torque resistance

in the upper stages of installation. The compression tests of the two medium-dense screw pile designs (U1MD and U2MD) resulted in structural failure (Figure 12a) of the lower helix of each pile through the upwards bending of the helix, highlighting the difficulty in designing the helices with a large D_h/D_c ratio of 3. The compression tests of both the single (U1MD) and double-helix (U2MD) medium-dense screw pile designs achieved a displacement of 10% of the helix diameter or greater in both cases before failure of the helix was observed. It is at this level of displacement where the capacity is conventionally calculated, so although the U2MD design did not reach the maximum resistance before the failure occurred, the required data to calculate the in-service capacity was obtained. No helix bending was observed with the other piles during testing or on inspection after testing.

None of the test results from the six screw piles tested compared well with the predicted values (Q_{cp}) from the initial method adopted (Method 1c) to design the model screw piles, with the best prediction achieving just 74% of the observed value for pile U2VDA as shown in Figure 12b which presents the measured compressive capacity (Q_{cm}) normalised by the predicted values from Method 1c (Q_{cm}/Q_{cp}). This suggests that Method 1c is non-conservative for these modified pile geometries and that the N_q and/or K_{uc} values require further investigation.

Alternative compressive capacity prediction (Method 2c)

As the measured compressive capacity results from the centrifuge tests did not match the compressive capacity predictions from the initial design method (Method 1c), an alternative approach was considered in the analysis of the results to investigate the performance and suitability of the alternative method.

The compressive capacity design method suggested by Perko (2009) and supported by (BS 8004:2015, 2015) differs from Method 1c by imposing a limit on the bearing capacity factor (N_q) used in calculating the resistance from the pile tip and helices, similar to the idea of 'critical-depth' in straight-shafted pile design (Tavenas, 1971, Meyerhof, 1976), which is no longer supported (Fleming et al., 2009) as this is related to dilation suppression which would not be appropriate for shallow screw piles. Perko (2009) calculates bearing capacity factor using Meyerhof (1951) equations, corrected for shape and depth by formulae proposed by Hansen (1970) and Vesic (1973). Based on experience, Perko (2009) limits the corrected N_q values to a maximum value as determined at a depth of $2D_{ha}$. In Method 1c, the N_q values were not limited with depth, but in Method 2c which follows Perko (2009), N_q was limited as prescribed to test this affect. Compressive shaft resistance and cylindrical-shear resistance values were calculated as directed by Perko (2009) and as in Method 1c. Predictions made for all pile designs using the Perko (2009) method (Method 2c) are compared against the measured values in Figure 13, where it is evident that the approach provides a good match with the measured compressive capacity values in the very-dense designs (U2VD, O2VD, U1VD-A, U1VD-B). However, this is not the case in the two medium-dense tests where the measured capacities are equal to 56% and 75% of the predicted loads.

Proposed compressive capacity prediction (Method 3c)

Based upon the poor performance of the compressive capacity predictions from Methods 1c and 2c, further analyses were conducted using previous research on continuous helical displacement (CHD) piles (Jeffrey, 2016) to improve the predictions (resulting in Method 3c). Jeffrey et al. (2016) obtained bearing capacity factor values, from deconvolution of instrumented CHD piles (cast-insitu type screw piles), which differed from those proposed by Berezantzev (1961). The overprediction of the compressive capacity of the screw piles from both Method 1c and 2c was suspected to be related to the bearing capacity factors used in the calculation of the compressive resistances generated by the pile tip and lowermost helix. To

investigate this, firstly the soil-soil and soil-steel shaft resistances, calculated from Equations (6) and (7) with the same soil properties and lateral earth pressure used in Method 1c, were subtracted from the total measured capacity to give the contribution from the bearing areas of the pile tip and lowermost helix. The calculated contribution of the steel-soil shaft resistance to the total compressive capacity was found to be low for each pile design. For example, the shaft of pile U1VD-B ($H/D_h = 7.33$) contributed 10.5% to the total capacity, as calculated with Equation (7) or 0.09MPa in terms of shaft resistance. This value is in line with centrifuge tests by Urabe et al. (2015) of a compressively loaded 480mm core diameter, wing-tip pile installed into very-dense sand to an H/D_h of 7.14. From their instrumented piles, Urabe et al. (2015) reported a shaft contribution ranging from 5.9 to 10.8% (up to 0.05MPa shaft resistance) of the total capacity for their 1W2.1 pile. Field data from Gavin et al. (2014) of a single-helix screw pile ($D_c = 110\text{mm}$, $D_h = 400\text{mm}$, $H/D_h = 6$) showed 0.06MPa of shaft resistance during compressive loading. Discrete Element Modelling (DEM) of the O2VD pile by Sharif et al. (2019) and the other pile designs in this paper also demonstrates that the total shaft contribution to the compressive capacity is approximately 8%.

The bearing capacity factor, N_q , was then back-calculated for each of the pile designs using the relationship in Equation (8). These calculated N_q values agree well with those determined by Jeffrey et al. (2016) in a study of continuous helical displacement (CHD) piles, as shown in Figure 14. Jeffrey et al. (2016) investigated a type of cast-insitu pile where the split between shaft and base capacity and the applicability of the approach was verified by strain gauge instrumentation placed within the model pile. This study was used as the reference for the analysis adopted here as the CHD process involves the full displacement penetration of a relatively large flighted bullet device into the soil in a perfect pitch matched manner. The bullet device is then reversed in a similar perfect manner with concrete injection to form the final pile and maintain the stress and strain regime in the ground associated with the bullet penetration. The approach was adopted as a basis for analysis due to its general similarities with the screw pile process and was previously used to determine screw pile performance by Al-Baghdadi (2018). Jeffrey et al. (2016) showed that enhanced shaft capacity is obtained in these rotationally installed full displacement techniques resulting in a greater share of resistance being associated with the shaft than the tip and the need to use reduced values with respect to the approach proposed by Berezantsev et al. (1961). Using the empirical relationship (Equation (13)) proposed by Jeffrey et al. (2016) between N_q and peak friction angle (Table 4), with Equation (5) for the lateral earth pressure coefficient used in the calculation of the shaft resistance (also used by Perko (2009) and Jeffrey et al. (2016)), a third method (Method 3c) is proposed to calculate the compressive capacity of the screw piles. The results of Method 3c, included in Figure 13, provide a much closer match to the measured values with an average measured to predicted capacity ratio (Q_{cm}/Q_{cp}) of 0.98. The advantage of the proposed method (Method 3c) over the previously discussed methods (1c and 2c) is most apparent in the medium-dense designs where the measured to predicted capacity ratios (Q_{cm}/Q_{cp}) are equal to 0.79 and 0.83 for piles U1MD and U2MD respectively.

The area of cylindrical shear between the helices of the optimised O2VD pile is 10.4 % less than the non-optimised U2VD design. Whereas, the area of the lower helix (including the pile tip) of O2VD is 37.9 % less than U2VD. Thus, since the combined surface area of the lower helix and assumed plugged pile tip generate the majority of the compressive resistance of a screw pile, the reliable calculation of the bearing capacity factor is critically important. The proposed Method 3c, using the revised N_q calculation from Equation 13 gave a measured to predicted compressive capacity ratio of 1.07 which is a significant improvement over the initial Method 1c ratio of 0.68.

$$N_q = 1.33e^{0.11\phi'_{pk}} \quad (13)$$

Tensile Capacity Tests

The results of tensile loading on the piles are shown in Figure 15a, with the ultimate tensile capacity defined as the value at a displacement of $0.1D_{ha}$. Predictions of the tensile capacity (Q_{tp}) from the Das and Shukla (2013) based Method 1t used in the initial design process are 34 to 77% lower than the measured loads (Q_{tm}) (Table 8 and Figure 15b) in the very-dense sand (U2VD, U1VD-A, U1VD-B, and O2VD). Evaluation of piles U2VD and U1VD-B (Figure 15a) shows that they have very similar uplift capacity, suggesting a relatively deep single helix ($H_n/D_{hn} = 7.35$) in a non-optimised form is more efficient in terms of tensile loading and installation requirements and the inclusion of the second helix ($H_n/D_{hn} = 5.35$) is not justified.

The optimised pile (O2VD) again under performs with the changes in cross section and helix diameter having a negative effect on tensile capacity (24.4% less than non-optimised U2VD). A similar conclusion can be drawn from the results of the two tensile tests in the medium-dense sand, in that there is little benefit in the addition of a second helix in terms of either tensile capacity, which is not significantly improved, or installation requirements (Figure 9), which increase with the presence of the second helix. The results in Figure 15 highlight that although the ultimate capacity of pile U2MD appears to be in line with the other pile tests, the stiffness is greatly reduced in comparison to the other piles, indicating that this test may have been compromised through elastic deformation of the helical plates from the vertical force experienced during installation. No visible damage to the pile was apparent after the test, but the large helices may have experienced elastic deformation during installation, creating a pre-strained system that was more pliable on initial loading in the upwards direction.

Alternative tensile capacity prediction (Method 2t)

Since the predicted tensile capacity from Method 1t did not match the measured tensile capacity, an alternative method was again investigated. Figure 16 presents measured versus predicted tensile capacities using the method prescribed by Perko (2009), termed Method 2t. Perko (2009) calculates the tensile capacity as per the compressive capacity, but applies a global factor of 0.87 to the calculated capacity on account of disturbance caused during installation. The Perko (2009) approach differs from Method 1t in the way in which the shallow failure wedge contributes to the capacity. Instead of varying the wedge with the soil friction angle, the wedge defined by Perko (2009) has a fixed angle of 45° from vertical, only includes the weight of soil and neglects friction on the failure surface (i.e. between the uplifting wedge and the undisturbed soil). As evident in Figure 16 and Table 8, the predictions from this method were also significantly greater than the measured values with over-predictions of 36 to 63%.

Alternative tensile capacity prediction (Method 3t)

As the previous methods (1t and 2t) did not provide satisfactory estimates of tensile capacity in the very-dense designs, an alternative approach was used for the tensile design of the medium-dense piles (U1MD and U2MD). The results from the very-dense tests were compared with a large number of plate and screw anchor uplift simulations using FEA by Cerfontaine et al. (2018), from which the relationship in Equation (14) was derived as a best-fit line through tests in medium-dense sand with friction angles of $38 - 41^\circ$ ($\phi = 40.4^\circ$ for HST95 at $D_r = 57\%$ (Table 4)). This uplift capacity was calculated as part of the design process previously outlined to create the medium-dense screw pile designs shown in Figure 5.

$$N_{\gamma} = 0.5226 \left(\frac{H}{D_h} \right)^2 + 1.6675 \frac{H}{D_h} \quad (14)$$

The uplift factors for the chosen designs were equal to 19.24 and 11.06 for the single (U1MD) and double-helix (U2MD) designs respectively. Although these are significantly lower than previously employed uplift factors, Q_{tm}/Q_{tp} was still much less than unity at 0.55 and 0.56 for the single and double-helix designs respectively (Figure 15b) and suggests that the plate anchor uplift factors only perform marginally better than Das and Shukla (2013). This over-prediction by a factor of two is also in line with findings reported in Schiavon et al. (2016), who attribute the over prediction to disturbance caused by installation and by Giampa et al. (2017) with their proposal that the failure wedge angle should be defined by the peak dilatancy angle of the soil which is more in line with the behaviour observed by Cheuk et al (2008) for pipeline uplift and Zhang et al. (2018) for the uplift of plates in sand. Although it should be noted that the inclination of this failure envelope may be influenced by control of the installation process where Kulhawy (1985) adopted a vertical failure plane to allow for significant disturbance above the top helix.

Proposed tensile capacity prediction (Method 4t)

An improved procedure for tensile design can be obtained by defining the uplift wedge angle as equal to the soil dilation angle, a change further supported by the Finite Element Analysis (FEA) in Cerfontaine et al. (2019a) as well as by Cheuk et al (2008), Zhang et al. (2018) and Giampa et al. (2017). Cerfontaine et al. (2019a) investigated the failure mechanism generated by the model screw piles reported herein. The results which showed an angle of the failure plane of 17° and 10.25° to the vertical for the very-dense and medium-dense conditions respectively (Cerfontaine et al., 2019a). These values are approximately equal to the dilatancy values for HST95 sand at the respective relative densities (Lauder et al., 2013). Furthermore, based upon the FEA by Cerfontaine et al. (2019b), which incorporates installation effects on the soil properties through step-wise loading at discrete depth intervals, it is suggested that the lower portion of the inclined failure surface above the uppermost helix (a distance $1.5D_h$ and $2.5D_h$ in very-dense and medium-dense sand, respectively) reflects a mobilised shear strength associated with post-peak behaviour and tending towards critical state, whilst further up the failure surface the shearing is initially in a pre-peak situation. Therefore, in calculating the shear resistance along the failure plane (at an angle from vertical equal to the dilation angle of the soil), in the lower section of the failure surface, the lateral earth pressure is assumed to equal K_{uc} (Equation (5)) and the friction angle on the failure plane equal to that at critical state (32°). For the remainder of the failure surface the at-rest lateral earth pressure coefficient and peak friction angles are used (see Cerfontaine et al. (2019b) for more detail). The shear resistance on the wedge failure surface plus the weight of the soil cone and the cylindrical shear resistance (in the case of the double-helix designs) were combined to give the total pull-out capacity for each pile. The cylindrical shear resistance was calculated with Equation (1) as per Perko (2009) for multi helix piles. The ratio of measured to predicted capacities from this process (Method 4t) (Figure 16) suggest an improved approach to design with Q_{tm}/Q_{tp} averaging 0.91 (0.99 with pile U2MD excluded). This method performs very well for all piles except U2MD, for which the capacity is over-predicted by 41% which is similar to that of the other calculation methods discussed. It is suggested that this poor prediction is due to the deformation of the pile during installation and testing.

From the FEA (Cerfontaine et al. (2019a and b) and centrifuge modelling herein it is suggested that inclusion of the second helical plate, for the geometry and helix plate depths adopted here, limits the size of the wedge uplift mechanism and the additional contribution from the cylindrical-shear mechanism is not as great as can be achieved from a deeper wedge mechanism as found for the single helix pile. Therefore, based upon the investigation of tensile capacity and mechanisms (for the H/D_h range of 2.83 to 7.35 investigated and reported herein), using more than one helix is not justified in terms of tensile uplift capacity (Figure 15) or the additional installation effort for the pile geometries investigated in this study. Lutenecker (2011) suggests that in tension two widely spaced helix plates may give better individual performance. This though suggests that there is greater scope for optimisation of screw piles for offshore applications and a particular pile design may have to be developed for each application depending on the relative magnitude of the tension and compression load requirements.

Conclusions

Six single and double helix screw piles designed for a single offshore loading case in very-dense and medium-dense sand have been installed using pitch matched parameters and tested in a geotechnical centrifuge for installation torque and load, compressive capacity and tensile capacity.

Very high installation torques and corresponding vertical forces were measured, with the medium-dense sand designs proving worse due to the larger core diameter required. An “optimized” design in which the core diameter was reduced near the pile tip was able to reduce installation loads significantly in very-dense sand, but was not able to provide the required axial capacity. Existing analytical and CPT-based torque prediction methods were found to perform poorly with respect to measured values while the CPT-torque correlation proposed by Davidson et al. (2018a) provided a close match for both torque and vertical force for all screw pile designs.

In all cases, the axial capacity in both tension and compression did not meet the predicted loads using published existing design methods. Alternative bearing capacity factors derived from CHD pile tests were found to perform better than factors derived in the screw pile literature for compressive capacity. Numerical analysis by Cerfontaine et al. (2019a and b) provided insight into the failure mechanisms of the screw pile designs under tensile loading. This information was used to modify previous design methods to provide a more accurate prediction of the tensile capacity.

The results also reveal that the inclusion of a second helix does not provide a significant advantage in terms of the compressive and tensile axial performance compared to an appropriately-designed single helix pile for the depth of installation adopted here.

Furthermore, the double-helix designs generate more installation force and torque and therefore it is recommended that single-helix designs are utilised. It is likely that further reductions in installation forces will be necessary and thus groups of smaller screw piles at each corner of a jacket structure may be a more feasible option for employing screw piles in the offshore wind energy sector where pitch matched installation is used. Large single screw piles may however be suitable for shallower water depths where the induced in-service axial forces are smaller.

Analysis of the measured installation torque and axial capacity data reveals that non-unique values of the empirical torque-capacity correlation factor (K_t), proposed by Hoyt and Clemence (1989), are possible for the same shaft diameter. Lutenecker (2019) also highlights that K_t values are often assumed to be unique regardless of the number of helices. A non-unique K_t value (for both tension and compression) contradicts both the K_t relationship

proposed by Hoyt and Clemence (1989), who suggested a unique value of K_t in tension, and the K_t to shaft diameter correlation proposed by Perko (2009). However, the value of K_t does appear to decrease with increasing shaft diameter, in line with previous research (e.g. Perko (2009)). The K_t correlation is widely used in industry to predict and verify the axial capacity of screw piles from the final installation torque values. Applying this relationship, which does not depend on critical screw pile design factors such as, the number of helices, to the large diameter screw piles presented in this paper would lead to a significant over-estimation of the tensile capacity and under-estimation of the compressive capacity.

Acknowledgements

The authors would like to acknowledge the support of EPSRC (Grant no. EP/N006054/1: Supergen Wind Hub Grand Challenges Project: Screw piles for wind energy foundations). This project has also received support from the European Union's Horizon 2020 research and innovation programme under the Marie Skłodowska-Curie grant agreement No 753156. The fourth author would like to acknowledge the financial support of the Iraqi Ministry of higher Education of Scientific Research (MOHESR). Elements of this work were undertaken using facilities developed as part of the ERDF-funded Scottish Marine & Renewables Test Centre (SMART) at the University of Dundee.

Appendix A

Al-Baghdadi et al. (2017b) equations for installation torque prediction from CPT cone resistance data.

$$T = T_s + T_b + T_h \quad A1.$$

$$T_s = aq_{ca} \tan \delta \pi L \frac{D_c^2}{2} f_1 \quad A2.$$

$$T_b = \frac{q_b \pi D_c^3}{12} \tan \delta f_2 \quad A3.$$

$$T_h = T_{h1} + T_{h2} + T_{h3} \quad A4.$$

$$T_{h1} = aq_{ca} \tan \delta \frac{\pi(D_h^3 - D_c^3)}{12k_0} \quad A5.$$

$$T_{h2} = aq_{ca} t \tan \delta \frac{\pi D_h^2}{2} \quad A6.$$

$$T_{h3} = q_{ca} t \frac{D_h^2 - D_c^2}{8} \quad \text{A7.}$$

$$k_0 = 1 - \sin \phi_{crit} \quad \text{A8.}$$

where T is the total torque which includes contributions from the shaft area (T_s), base of the pile core (T_b) and the helix (T_h), which has three components - T_{h1} from the underside of the helix, T_{h2} associated with the circumferential edge and T_{h3} from the leading or cutting edge of the helix. The earth pressure at rest term (K_0) uses the critical state friction angle and q_{ca} is the average q_c over a distance of $\pm 1.5 D_h$ from the depth of the helix in question. The pile end bearing resistance q_b was taken as $0.6 q_{ca}$ and the stress drop index (a) assumed to be 0.03 after Lehane et al. (2005). Al-Baghdadi et al. (2017b) also proposed that a rotation reduction factor was required for the shaft and base components ($f_1 = 0.75$ and $f_2 = 0.7$, respectively) for torque prediction after work by Deeks and White (2008). Al-Baghdadi (2018) also suggested that the stress drop index and rotation reduction factors were related to relative density.

Appendix B

Davidson et al. (2018a) equations for installation torque prediction from CPT cone resistance data.

$$T = T_s + T_b + \sum_1^n T_{h(n)} \quad \text{B1.}$$

$$T_h = T_{h1} + T_{h2} + T_{h3} \quad \text{B2.}$$

$$T_s = \sum_{\Delta x=1}^{\Delta x=L} a q_{ca} \tan \delta_{crit} \pi \Delta x \frac{D_c^2}{2} \quad \text{B3.}$$

$$T_b = q_{ca} \tan \delta_{crit} \pi \frac{D_c^3}{12} \quad \text{B4.}$$

$$T_{h1} = a q_{ca} \tan(\delta_{crit} + \theta) \frac{D_h^3 - D_c^3}{12 k_0} \quad \text{B5.}$$

$$T_{h2} = a q_{ca} \tan \delta_{crit} \pi t \frac{D_h^2}{2} \quad \text{B6.}$$

$$T_{h3} = a q_{ca} t \frac{D_h^2 - D_c^2}{4} \quad \text{B7.}$$

$$a = \frac{F_r}{\tan \delta_{crit}} \quad \text{B8.}$$

$$k_0 = 1 - \sin \phi_{crit} \quad \text{B9.}$$

$$\theta = \tan^{-1} \left(\frac{p}{\pi(D_h - D_c)} \right) \quad \text{B10.}$$

Appendix C

Equations for installation force prediction from CPT cone resistance data from Al-Baghdadi (2018).

$$F_v = F_s + F_b + \sum_1^n F_{h(n)} \quad \text{C1.}$$

$$F_s = \sum_{\Delta x=1}^{\Delta x=L} a q_{ca} \tan \delta_{crit} \pi D_c L f \quad \text{C2.}$$

$$F_b = q_{ca} \pi \frac{D_c^2}{4} f \quad \text{C3.}$$

$$F_h = F_{h1} + F_{h2} + F_{h3} \quad \text{C4.}$$

$$F_{h1} = a q_{ca} \pi \frac{D_h^2 - D_c^2}{4 k_0} \quad \text{C5.}$$

$$F_{h2} = a q_{ca} t \pi \frac{D_h}{k_0} \quad \text{C6.}$$

$$F_{h3} = q_{ca} t \frac{D_h - D_c}{2} \quad \text{C7.}$$

Notation

A	Stress drop coefficient
A_h	Area of helical plate
B	Cone penetrometer shaft diameter
D_{10}	Effective soil particle diameter
D_{50}	Average soil particle diameter
D_c	Pile core diameter
D_h	Helix diameter
D_{ha}	Average helix diameter
D_{hn}	Uppermost helix diameter
D_{hl}	Lowermost helix diameter

D_r	Relative density
f	Rotation reduction factor
f_1	Rotation reduction factor for pile shaft
f_2	Rotation reduction factor for pile tip
F_b	Installation force from pile tip
F_h	Installation force from helix
F_q	Bearing capacity factor in uplift from Das & Shukla (2013)
F_s	Installation force from pile shaft
F_v	Vertical installation force of screw pile
g	Acceleration due to Earth's gravity
H	Helix depth
H_l	Depth of lowermost helix
H_n	Depth of uppermost helix
k_0	At-rest earth pressure coefficient
K_p	Passive earth pressure coefficient
K_u	Post screw pile installation earth pressure coefficient for uplift
K_{uc}	Post screw pile installation earth pressure coefficient for compression
L	Length of screw pile shaft
m	Shape coefficient in relationship between ϕ and K_u
N_q	Bearing capacity factor
N_γ	Uplift factor for screw anchors and plates
p	Helix pitch
q_b	Pile tip bearing capacity
q_c	CPT cone resistance
q_{ca}	Average CPT cone resistance over a distance of $\pm 1.5D_h$
Q_{cm}	Measured compressive capacity
Q_{cp}	Predicted compressive capacity
$Q_{c,helix}$	Helix bearing capacity
$Q_{c,tip}$	Pile tip bearing capacity
Q_s	Shaft resistance
Q_{sc}	Cylindrical-shear resistance in compression
Q_{st}	Cylindrical-shear resistance in tension
Q_{tm}	Measured uplift capacity
Q_{tp}	Predicted uplift capacity
Q_u	Ultimate screw pile uplift capacity
S	Helix spacing
t	Helix plate thickness
T	Total torque
T_b	Torque from pile tip
T_h	Torque from helix
T_{h1}	Torque from lower surface of helix
T_{h2}	Torque from outer perimeter of helix
T_{h3}	Torque from leading edge of helix

T_s	Torque from pile shaft
z	Depth below surface
ψ	Dilation angle
ϕ'_{pk}	Peak internal friction angle
ϕ'_{crit}	Critical state friction angle
δ'_{crit}	Critical state interface friction angle
δ	Interface friction angle
γ'	Effective unit weight of soil
ρ_{max}	Maximum density of soil
ρ_{min}	Minimum density of soil

References

- Al-Baghdadi TA (2018). *Screw piles as offshore foundations: Numerical & physical modelling*. PhD thesis, University of Dundee, Dundee, UK.
- Al-Baghdadi TA, Brown MJ & Knappett JA (2016). Development of an inflight centrifuge screw pile installation and loading system. In *3rd European Conference on Physical Modelling in Geotechnics (Eurofuge 2016)* (L Thorel, A Bretschneider, M Blanc and S Escofier (eds)). IFSTTAR, France, pp. 239–244.
- Al-Baghdadi TA, Brown MJ, Knappett JA & Al-Defae AH (2017a). Effects of vertical loading on lateral screw pile performance. In *Proceedings of the Institution of Civil Engineers - Geotechnical Engineering* **170(3)**, 259–272, <http://dx.doi.org/10.1680/jgeen>.
- Al-Baghdadi TA, Brown MJ, Knappett JA & Ishikura R (2015). Modelling of laterally loaded screw piles with large helical plates in sand. In *3rd International Symposium on Frontiers in Offshore Geotechnics* (V Meyer (ed.)). Taylor & Francis Group, London, pp. 503–508.
- Al-Baghdadi TA, Brown MJ, Davidson C, Knappett JA, Brennan AJ, Wang L, Coombs WM, Augarde, CE, Richards D & Blake A (2017b). CPT based design procedure for installation torque prediction for screw piles installed in sand. In *8th International Conference on Offshore Site Investigation & Geotechnics (SUT OSIG)*. London, UK, vol. 1, pp. 346–353.
- Al-Defae AH, Caucis K & Knappett JA (2013). Aftershocks and the whole-life seismic performance of granular slopes. *Géotechnique* **63(14)**, 1230–1244.
- Baldi G, Bellotti R, Ghionna V, Jamiołkowski M & Pasqualini E (1986). Interpretation of CPTs and CPTUs; 2nd part: drained penetration of sands. In *Fourth International Geotechnical Seminar*. Nanyang Technological Institute, Singapore, pp. 143–156.

- Beatrice Offshore Windfarm Ltd (2017). Beatrice Offshore Wind Farm Piling Strategy. Beatrice Offshore Windfarm Ltd, UK. See <https://www2.gov.scot/Topics/marine/Licensing/marine/scoping/Beatrice/piling> (accessed 07/03/2018).
- Berezantsev VC, Khristoforov V & Golubkov V (1961). Load bearing capacity and deformation of piled foundations In *Proceedings of 5th International Conferences on Soil Mechanics and Foundation Engineering*. Paris, France, vol. 2, pp. 11–12.
- Bolton MD, Gui MW, Garnier J, Corte JF, Bagge G, Laue J & Renzi R (1999). Centrifuge cone penetration tests in sand. *Géotechnique* **49**(4): 543–552, <https://doi.org/10.1680/geot.1999.49.4.543>.
- Bruns B, Stein P, Kuhn C, Sychla H & Gattermann J (2014). Hydro sound measurements during the installation of large diameter offshore piles using combinations of independent noise mitigation systems. In *INTER-NOISE and NOISE-CON Congress and Conference Proceedings*. Institute of Noise Control Engineering, Melbourne, Australia, vol, 249, pp. 5629-5638.
- BSI (2015) BS 8004:2015. Code of practice for foundations. BSI, London, UK.
- Byrne B, Mcadam R, Burd H, Houlsby G, Martin C, Beuckelaers W, Zdravkovic L, Taborda D, Potts D, Jardine R, Ushev E, Liu T, Abadias D, Gavin K, Igoe D, Doherty P, Gretlund JS, Andrade MP, Wood AM, Schroeder F, Turner S & Plummer M (2017). PISA: New Design Methods for Offshore Wind Turbine Monopiles. In *8th International Conference on Offshore Site Investigation & Geotechnics (SUT OSIG)*. London, UK, vol. 1, pp. 142–156.
- Byrne BW & Houlsby GT (2015) Helical piles: an innovative foundation design option for offshore wind turbines. *Philosophical Transactions of the Royal Society A* **373**(2035), <https://doi.org/10.1098/rsta.2014.0081>.
- Cerfontaine B, Knappett JA, Brown MJ & Bradshaw AS (2018) Effect of soil deformability on the failure mechanism of shallow plate or screw anchors in sand. *Computers and Geotechnics* **109**: 34–45, <https://doi.org/10.1016/j.compgeo.2019.01.007>.
- Cerfontaine B, Knappett JA, Brown MJ & Bradshaw AS (2019a). Design of plate and screw anchors in dense sand: failure mechanism, capacity and deformation. In *7th International Symposium on Deformation Characteristics of Geomaterials (IS-*

- Glasgow 2019*) (A Tarantino & E Ibraim (eds)). E3S Web of Conferences, EDP Sciences, pp. 1–6, <https://doi.org/10.1051/e3sconf/20199216010>.
- Cerfontaine B, Brown MJ, Knappett JA and Davidson C, (2019b). Finite element modelling of the uplift behaviour of screw piles in sand. In *Proceedings of the 1st International Symposium on Screw Piles for Energy Applications (ISSPEA 2019)* (C Davidson, MJ Brown, JA Knappett, AJ Brennan, CE Augarde, L Wang, WM Coombs, D Richards, D White, & A Blake (eds)). University of Dundee, Dundee, UK, pp.69–75. <https://doi.org/10.20933/100001123>.
- Cheuk CY, White DJ and Bolton MD (2008). Uplift mechanisms of pipes buried in sand. *Journal of Geotechnical Geoenvironmental Engineering* **134**(2): 154–163.
- Das BM & Shukla SK (2013) *Earth anchors*. J Ross Publishing, USA.
- Davidson C, Al-Baghdadi TA, Brown MJ, Knappett JA, Brennan AJ, Augarde CE, Coombs WM, Wang L, Richards D, Blake A & Ball J (2018a) A modified CPT based installation torque prediction for large screw piles in sand. In *Proceedings of the 4th International Symposium CPT'18 - Cone Penetration Testing* (MA Hicks, F Pisanò, J Peuchen (eds)). CRC Press, Leiden, The Netherlands, pp. 255–261, <https://doi.org/10.1201/9780429505980>.
- Davidson C, Al-Baghdadi TA, Brown MJ, Knappett JA, Brennan AJ, Augarde CE, Coombs WM, Wang L, Richards D, Blake A & Ball J (2018b) Centrifuge modelling of optimised screw piles for offshore wind energy foundations. In *Proceedings of the 9th International Conference on Physical Modelling in Geotechnics (ICPMG 2018)* (A McNamara, S Divall, R Goodey, N Taylor, S Stallebrass, J Panchal (eds)). Taylor and Francis, pp. 695–700, <https://doi.org/10.1201/9780429438646>.
- Deeks AD (2008) *An investigation into the strength and stiffness of jacked piles in sand*. PhD thesis. University of Cambridge, Cambridge, UK.
- Deeks AD and White D (2008) Centrifuge modelling of rotary-jacked tubular piles: gyropiling. In *Proceedings of the 2nd BGA International Conference on Foundations (ICOF 2008)* (MJ Brown, MF Bransby, AJ Brennan, and JA Knappett (eds)). IHS BRE Press, vol. 2, pp. 532–544.
- DNV (2007) Recommended Practice DNV-RP-C205: Environmental Conditions and Environmental Loads. Høvik, Norway, DNV.

- DNV (2010) DNV-OS-J101: Design of Offshore Wind Turbine Structures. Høvik, Norway, DNV.
- Elsherbiny, ZH & MH El Naggar (2013). "Axial compressive capacity of helical piles from field tests and numerical study." *Canadian Geotechnical Journal* **50(12)**: 1191-1203.
- Fleming K, Weltman A, Randolph M & Elson K (2009) *Piling engineering*. Abingdon, UK, Taylor and Francis.
- Garcia-Galindo P (2017) *Installation behaviour of open and close ended piles in sand while applying torque*. MSc thesis. University of Dundee, Dundee, UK.
- Garcia-Galindo P, Davidson C & Brown MJ (2018) Installation behavior of open ended and closed ended piles with torque application. *Proceedings of the 1st International Conference on Press-in Engineering 2018*. International Press in Association, Japan. pp. 379–386.
- Garnier J, Gaudin C, Springman S, Culligan P, Goodings D, Konig D, Kutter B, Phillips R, Randolph M & Thorel L (2007) Catalogue of scaling laws and similitude questions in geotechnical centrifuge modelling. *International Journal of Physical Modelling in Geotechnics* **7(3)**: 01–23.
- Gavin K, Doherty P, & Spagnoli G (2013) Prediction of the installation torque resistance of large diameter helical piles in dense sand. In *Proceedings of 1st International Geotechnical Symposium of Helical Foundations*. International Society for Helical Foundations, University of Massachusetts, Amherst, USA, pp. 578 – 585.
- Gavin K, Doherty P, & Tolooitan A (2014) Field investigation of the axial resistance of helical piles in dense sand. *Canadian Geotechnical Journal* **51(11)**: 1343–1354.
- Ghaly A & Hanna A (1991) Experimental and theoretical studies on installation torque of screw anchors. *Canadian Geotechnical Journal* **28(3)**: 353–364.
- Ghaly A, Hanna A & Hanna M (1991) Uplift behavior of screw anchors in sand I: dry sand. *Journal of Geotechnical Engineering* **117**: 773–793.
- Giampa JR, Bradshaw AS & Schneider JA (2017) Influence of Dilation Angle on Drained Shallow Circular Anchor Uplift Capacity. *International Journal of Geomechanics* **17(2)**: 04016056-1–04016056-11.
- Golightly C (2014) Technical Paper: Tilting of monopiles Long, heavy and stiff; pushed beyond their limits. *Ground Engineering* January 2014: 20–23.

- Hansen JB (1970) *A revised and extended formula for bearing capacity*. Copenhagen, Denmark, Danish Geotechnical Institute.
- Huisman M (2019) Silent foundation concept: helical piles for skirt and pre-piled jacket foundations. In *Proceedings of the 1st International Symposium on Screw Piles for Energy Applications (ISSPEA 2019)* (C Davidson, MJ Brown, JA Knappett, AJ Brennan, CE Augarde, L Wang, WM Coombs, D Richards, D White, & A Blake (eds)). University of Dundee, Dundee, UK, pp.117–118.
<https://doi.org/10.20933/100001123>.
- Hoyt RM & Clemence SP (1989) Uplift capacity of helical anchors in soil. In *Proceedings of the 12th International Conference on Soil Mechanics and Foundation Engineering*. Taylor & Francis, Rio de Janeiro, Brazil, vol. 2, pp. 1019–1022.
- Jeffrey JR, Brown MJ, Knappett JA, Ball JD & Caucis K (2016) CHD pile performance: part I – physical modelling. *Proceedings of the Institution of Civil Engineers - Geotechnical Engineering* **169**(5): 421–435. <https://doi.org/10.1680/jgeen.15.00131>.
- Joint Nature Conservation Committee (JNCC) (2010) Statutory nature conservation agency protocol for minimising the risk of injury to marine mammals from piling noise. JNCC, Aberdeen, UK. See
http://archive.jncc.gov.uk/pdf/jncc_guidelines_piling%20protocol_august%202010.pdf (Accessed 30/09/19).
- Knappett JA, Brown MJ, Brennan AJ & Hamilton L (2014) Optimising the compressive behaviour of screw piles in sand for marine renewable energy applications. In *DFI/EFFC 11th International Conference on Piling and Deep Foundations*. Deep Foundations Institute, Stockholm, Sweden, Vol. IC-2014, 1904.
- Kulhawy FH (1985) Uplift Behavior of Shallow Soil Anchors—An Overview In *Proceedings of Uplift Behavior of Anchor Foundations in Soil* (Clemence SP (ed)). American Society of Civil Engineers, New York, NY, pp. 1-25.
- Lauder KD, Brown MJ, Bransby MF & Boyes S (2013) The influence of incorporating a forecutter on the performance of offshore pipeline ploughs. *Applied Ocean Research* **39**: 121–130. <https://doi.org/10.1016/j.apor.2012.11.001>.
- Leanwind (2013) *Summary description of LEANWIND 8 MW reference turbine*. See <http://www.leanwind.eu/>.

- Leblanc C, Houlsby GT & Byrne BW (2010) Response of stiff piles in sand to long-term cyclic lateral loading. *Géotechnique* **60(2)**: 79–90.
- Lehane BM, Schneider JA & Xu X (2005) The UWA-05 method for prediction of axial capacity of driven piles in sand. In *Frontiers in Offshore Geotechnics: Proceedings of the International Symposium on Frontiers in Offshore Geotechnics (IS-FOG 2005)*. (S Gourvenec, and M Cassidy (eds)) CRC Press, Perth, Australia, pp. 683–689.
- Li Z, Haigh SK & Bolton MD (2010) Centrifuge modelling of mono-pile under cyclic lateral loads. In *Proceedings of the 7th International Conference on Physical Modelling in Geotechnics*. (S Springman, J Laue and L Seward (eds)) CRC Press, Zurich, Switzerland, vol. 2, pp. 965–970.
- Lutenegger AJ (2011) Behavior of Multi-Helix Screw Anchors in Sand. In *14th Pan-American Conference on Soil Mechanics and Geotechnical Engineering 64th Canadian Geotechnical Conference*. ISSMGE.
- Lutenegger AJ (2019) Screw Piles And Helical Anchors – What We Know And What We Don't Know: An Academic Perspective – 2019. In Proceedings of the 1st International Symposium on Screw Piles for Energy Applications (ISSPEA 2019) (C Davidson, MJ Brown, JA Knappett, AJ Brennan, CE Augarde, L Wang, WM Coombs, D Richards, D White, & A Blake (eds)). University of Dundee, Dundee, UK, pp.15–28. <https://doi.org/10.20933/100001123>.
- Meyerhof GG (1951) The ultimate bearing capacity of foundations. *Géotechnique* **2(4)**: 301–332.
- Meyerhof GG (1976) Bearing Capacity and Settlement of Pile Foundations. *Journal of the Geotechnical Engineering Division, ASCE* **102(3)**: 197–228.
- Mitsch MP & Clemence SP (1985) The uplift capacity of helix anchors in sand. In *Uplift Behavior of Anchor Foundations in Soil*. (SP Clemence (ed)) American Society of Civil Engineers, New York, USA, pp. 26–47.
- Mohajerani A, Bosnjak D & Bromwich D (2016) Analysis and design methods of screw piles: A review. *Soils and Foundations* **56(1)**: 115–128.
- Morais TDSO & Tsuha CDHC (2014) A new experimental procedure to investigate the torque correlation factor of helical anchors. *Electronic Journal of Geotechnical Engineering* **19 (Bund. P)**: 3851–3864.

- Perko HA (2009) *Helical piles: a practical guide to design and installation*. Hoboken, USA, John Wiley & Sons.
- Phillips R & Valsangkar A (1987) *An experimental investigation of factors affecting penetration resistance in granular soils in centrifuge modelling*. Cambridge, UK, Technical Report No. CUED/D - Soils TR 210.
- Randolph M & Gourvenec S (2011) *Offshore Geotechnical Engineering*. Spon Press, Abingdon, Oxon, UK.
- Sakr M (2015) Relationship between installation torque and axial capacities of helical piles in cohesionless soils. *Canadian Geotechnical Journal* **52(6)**: 747–759.
- Schiavon JA, Tsuha CDHC & Thorel L (2016) Scale effect in centrifuge tests of helical anchors in sand. *International Journal of Physical Modelling in Geotechnics* **16(4)**: 185–196.
- Sharif Y, Brown MJ, Ciantia M, Knappett JA, Davidson C, Cerfontaine B, Robinson S & Ball J (2019) Numerically modelling the installation and loading of screw piles using DEM. In *Proceedings of the 1st International Symposium on Screw Piles for Energy Applications (ISSPEA 2019)* (C Davidson, MJ Brown, JA Knappett, AJ Brennan, CE Augarde, L Wang, WM Coombs, D Richards, D White, & A Blake (eds)). University of Dundee, Dundee, UK, pp.101–108. <https://doi.org/10.20933/100001123>.
- Spagnoli G (2016) A CPT-based model to predict the installation torque of helical piles in sand. *Marine Georesources & Geotechnology* **35(4)**: 578–575.
- Spagnoli G & Gavin K (2015) Helical piles as a novel foundation system for offshore piled facilities. In *Proceedings of the Abu Dhabi International Petroleum Exhibition and Conference*. Society of Petroleum Engineers, Abu Dhabi, UAE.
- Tappenden KM & Sego DC (2007) Predicting the axial capacity of screw piles installed in Canadian soils. In *Proceedings of OttawaGeo2007*. Canadian Geotechnical Society, Ottawa, Canada, pp.1608–1615.
- Tavenas FA (1971) Load tests results on friction piles in sand. *Canadian Geotechnical Journal* **8(1)**: 7–22.
- Tsuha CDHC & Aoki N (2010) Relationship between installation torque and uplift capacity of deep helical piles in sand. *Canadian Geotechnical Journal* **47(6)**: 635–647.
- Urabe K, Tokimatsu K, Suzuki H, & Asaka Y (2015) Bearing Capacity and Pull-Out Resistance of Wing Piles During Cyclic Vertical Loading. In *6ICEGE – Proceedings*

of the 6th International Conference on Earthquake Geotechnical Engineering,
Christchurch, New Zealand, pp.358-3675.

Vesic AS (1973) Analysis of ultimate loads of shallow foundations. *Journal of Soil Mechanics and Foundation Design* **99** (No. SM 1): 45–73.

Windeurope Business Intelligence (2017) *The European offshore wind industry: Key trends and statistics 2016*. See <https://windeurope.org/>.

Zhang D (1999). Predicting capacity of helical screw piles in Alberta soils. MSc thesis, University of Alberta, Edmonton, Canada.

Zhang X, Liu J & Liu M (2018) Experimental Study on Uplift Behavior of Group Anchors in Sand. *Geotechnical Testing Journal* **42** (no.3): 687-702.

Table 1. Aerodynamic and hydrodynamic properties for loading calculations.

Parameter	Value
Reference wind speed (m/s)	32
Reference wind speed elevation (mASL)	10
Air temperature [°C]	5
Kinematic viscosity of air at 5° (m ² /s)	13.60x10 ⁶
Density of air at 5°C (kg/m ³)	1.226
Significant wave height (m)	11.5
Wave period (s)	15
Storm Duration (hours)	3
Water temperature (°C)	5
Kinematic viscosity of water at 5°C (m ² /s)	1.56x10 ⁶
Density of sea water at 5°C (kg/m ³)	1027.6
Current speed (m/s)	0.5

Table 2. Values of m for various soil friction angles, as derived by Mitsch and Clemence (1985).

Soil friction angle, ϕ (°)	m
25	0.033
30	0.075
35	0.18
40	0.25
45	0.289

Table 3. Prototype model screw pile dimensions (m) with 1:80th scale model dimensions in brackets (mm). See Figure 5 for locations of dimensions.

Dimension	Screw Pile Model					
	U2VD	O2VD	U1VD-A	U1VD-B	U2MD	U1MD
Total length, L	13.00 (162.50)	13.00 (162.50)	10.24 (128.00)	13.00 (162.50)	18.00 (225.00)	16.00 (200.00)
Upper helix mid-depth, H_n	12.66 (158.30)	12.66 (158.30)	9.90 (123.80)	12.66 (158.30)	10.94 (136.80)	15.66 (195.80)
Helix spacing, S	3.40 (42.50)	3.40 (42.50)			6.72 (84.00)	
Helix pitch, p	0.56 (7.00)	0.56 (7.00)	0.56 (7.00)	0.56 (7.00)	0.56 (7.00)	0.56 (7.00)
Helix plate thickness, t	0.11 (1.40)	0.11 (1.40)	0.11 (1.40)	0.11 (1.40)	0.11 (1.40)	0.11 (1.40)
Upper helix diameter, D_{hn}	1.70 (21.25)	1.70 (21.25)	1.70 (21.25)	1.70 (21.25)	3.36 (42.00)	3.36 (42.00)
Lower helix diameter, D_{hl}	1.70 (21.25)	1.34 (16.75)			3.36 (42.00)	
Upper core diameter, D_c	0.88 (11.00)	0.88 (11.00)	0.88 (11.00)	0.88 (11.00)	1.12 (14.00)	1.12 (14.00)
Lower core diameter, D_{cl}		0.60 (7.50)				
Upper core length, L_u		8.22 (102.75)				
Upper helix depth/diameter, H_n/D_{hn}	5.35	5.35	5.82	7.35	2.83	4.17
Lower helix depth/diameter H_l/D_{hl}	7.35	9.33			4.85	

Table 4. HST95 sand material properties (Lauder, 2010, Al-Defae, 2013).

Property	Value
Effective particle size, D_{10} (mm)	0.09
Average particle size, D_{50} (mm)	0.14
Peak friction angle, ϕ'_{pk} (°) at 57% relative density	40.40
Peak friction angle, ϕ'_{pk} (°) at 84% relative density	45.80
Critical state friction angle, ϕ'_{crit} (°)	32
Sand-steel interface friction angle, δ'_{crit} (°)	24
Angle of dilation*, ψ (°)	16
Maximum dry density, ρ_{max} (kN/m ³)	17.58
Minimum dry density, ρ_{min} (kN/m ³)	14.59

*Inferred from best-fit peak strength relationship from direct shear tests for data at effective stresses between 50-200kPa and critical state friction angle, at 80% relative density (Al-Defae, 2013).

Table 5. Screw pile centrifuge testing programme. Peak friction angles calculated from relative density using relationship proposed by Al-Defae, (2013) for HST95 sand).

Test	Screw Pile	Test Type	Relative Density, D_r (%)	Peak Friction Angle, ϕ_{pk}
01-U2TVD	U2VD	Tension	83.4	45.7
02-O2TVD	O2VD	Tension	82.2	45.4
03-U2CVD	U2VD	Compression	84.6	45.9
04-O2CVD	O2VD	Compression	84.6	45.9
05-U1TVD-A	U1VD-A	Tension	84.7	45.9
06-U1CVD-A	U1VD-A	Compression	84.7	45.9
07-U1TVD-B	U1VD-B	Tension	82.7	45.5
08-U1CVD-B	U1VD-B	Compression	84.8	45.9
09-U1TMD	U1MD	Tension	56.0	40.2
10-U1CMD	U1MD	Compression	56.0	40.2
11-U2TMD	U2MD	Tension	58.5	40.7
12-U2CMD	U2MD	Compression	58.5	40.7

Table 6. Compression test results for comparison with the 32.31MN compressive design load.

Note: measured compressive capacity is defined at a displacement of $0.1D_{ha}$.

Pile	Test	Measured (MN)	Measured/Predicted – Method 1c	Measured/Predicted – Method 2c	Measured/Predicted – Method 3c
U2VD	03-U2CVD	34.99	0.75	1.00	1.25
O2VD	04-O2CVD	20.96	0.68	0.94	1.07
U1VD-A	06-U1CVD-A	23.62	0.73	0.86	1.20
U1VD-B	08-U1CVD-B	23.63	0.57	0.83	0.92
U1MD	10-U1CMD	41.57	0.47	0.56	0.79
U2MD	12-U2CMD	67.26	0.57	0.69	0.88
Average			0.63	0.81	1.02

Table 7. Theoretical (Perko, 2009) and back-calculated torque-capacity correlation factors (K_t).

Screw Pile	Back-calculated Torque-Capacity values (Kt)		Theoretical values (Kt) Perko (2009)	Torque-Capacity $K_t = \frac{1433}{D_c^{0.92}}$ from
	Tension	Compression		
U2VD	1.58	4.67	2.80	
O2VD	1.44	3.19	3.98	
U1VDA	1.88	5.44	2.80	
U1VDB	1.89	5.05	2.80	
U1MD	1.45	3.16	2.24	
U2MD	0.79	2.73	2.24	

Table 8. Predicted and measured tensile capacities of all screw pile designs. Note: measured tensile capacity is defined at a displacement of $0.1D_{ha}$.

Pile	Test	Measured (MN)	Measured/Predicted Tensile Capacity			
			Method 1t	Method 2t	Method 3t	Method 4t
U2VD	02U2TVDB	11.76	0.66	0.64		1.00
O2VD	03O2TVD	8.89	0.52	0.52		1.07
U1VD-A	06U1TVDA	6.96	0.30	0.51		1.00
U1VD-B	18U1TVDB	11.31	0.23	0.52		0.93
U1MD	21U1TMD	14.69	0.32	0.37	0.53	0.95
U2MD	23U2TMD	14.47	0.60	0.43	0.55	0.59
Average			0.44	0.50		0.91

Figure captions

Figure 1. Schematic of a screw pile and the typical terminology used with addition of potential failure mechanisms during loading in tension and compression.

Figure 2. Schematic of an 8MW offshore wind turbine and four-legged steel jacket (dimensions in metres unless otherwise stated).

Figure 3. Uplift breakout factors for various peak friction angles, based upon Das & Shukla (2013), with maximum values given as horizontal lines for deep failure mechanism cases.

Figure 4. Comparison of installation torque predictions from published methods.

Figure 5. Screw piles tested in centrifuge. See Table 3 for dimensions.

Figure 6. Centrifuge test data showing torque and force data for the duration of the installation and load test of screw pile U1VD-B in a) compression and b) tension. 1 = centrifuge spin up; 2 = installation; 3 = load test.

Figure 7. Cone penetration test data for medium-dense ($D_r = 52\%$) and very-dense ($D_r = 82\%$) dry HST95 sand at prototype scale.

Figure 8. Measured installation torque at prototype scale for all model screw piles.

Figure 9. Measured vs predicted installation torque for piles: a) U2VD, b) U1VD-B, c) O2VD and d) U1MD.

Figure 10. Measured installation force at prototype scale for all model screw piles.

Figure 11. Measured vs predicted installation force for piles: a) U2VD, b) U1VD-B, c) O2VD and d) U1MD.

Figure 12. a) Measured prototype compressive capacity test results, b) measured/predicted compressive capacity using Method 1c predictions. The asterix indicates the point of structural failure of the helix in piles U1MD and U2MD.

Figure 13. Measured vs predicted compressive capacity.

Figure 14. Back calculated bearing capacity factors (N_q) from single helix piles in this study and continuous helical displacement piles in Jeffrey et al. (2016).

Figure 15. a) Measured tension capacity test results, b) measured/predicted tensile capacity.

Figure 16. Measured vs predicted tensile capacity.

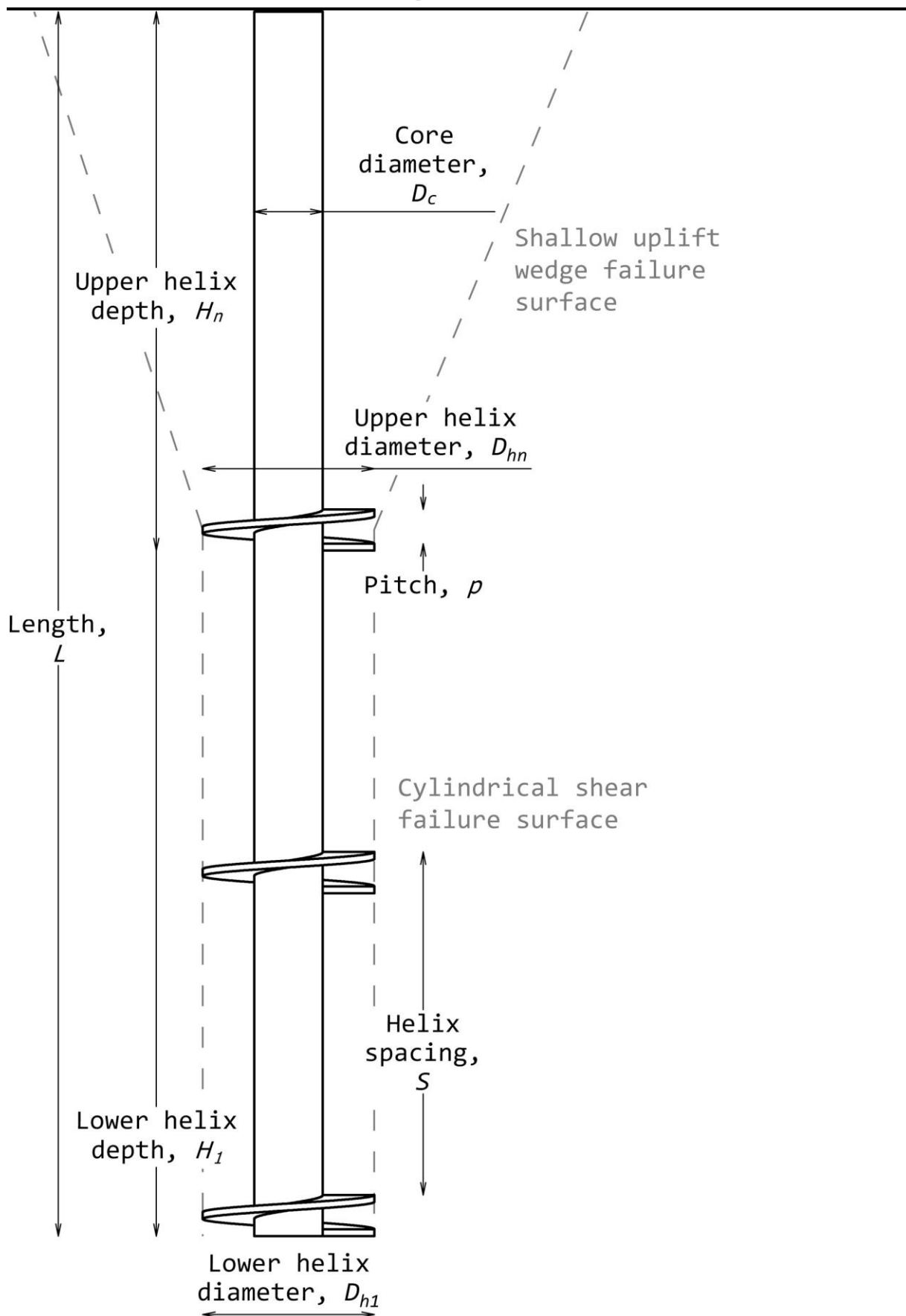


Figure 1. Schematic of a screw pile and the typical ter

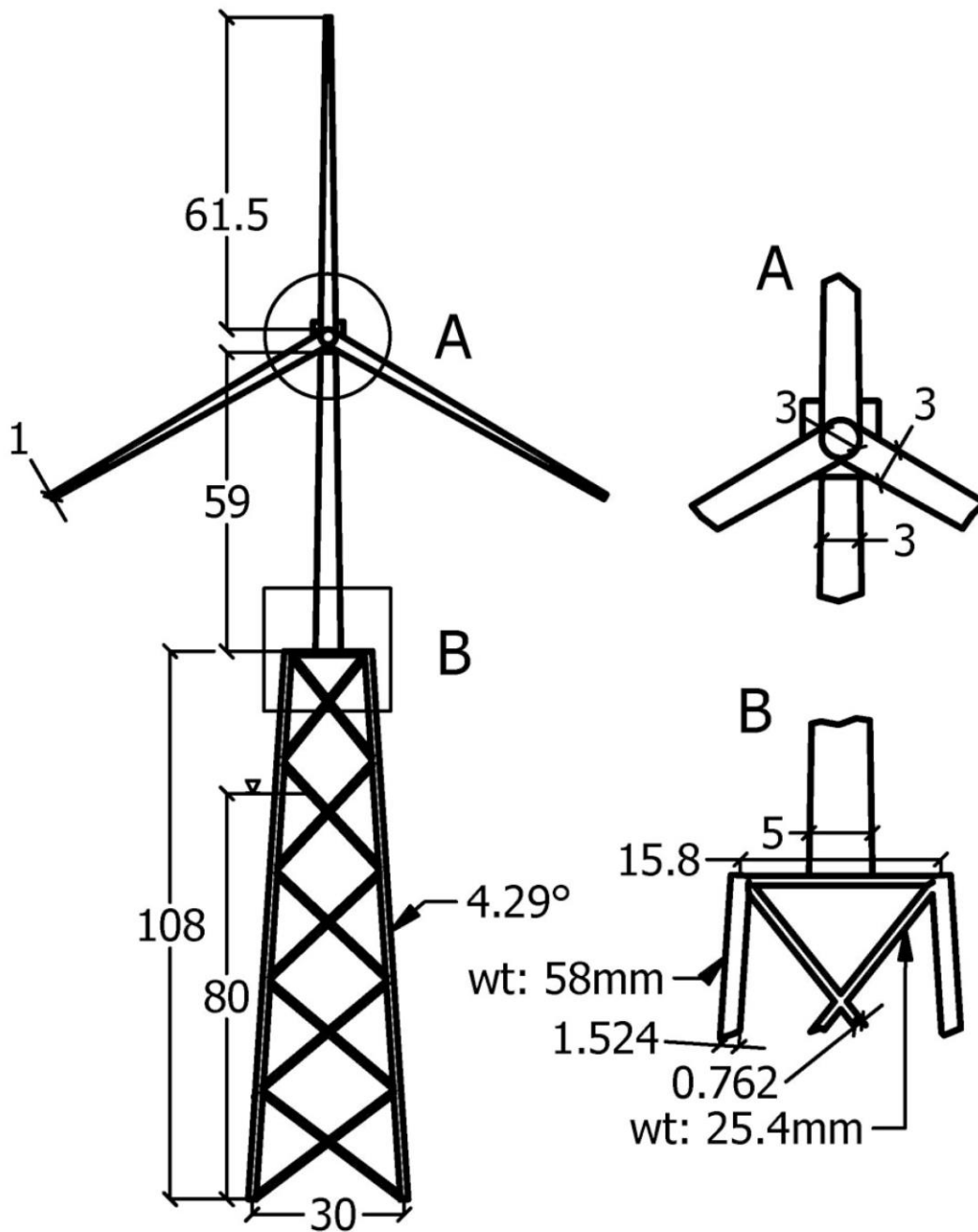


Figure 2

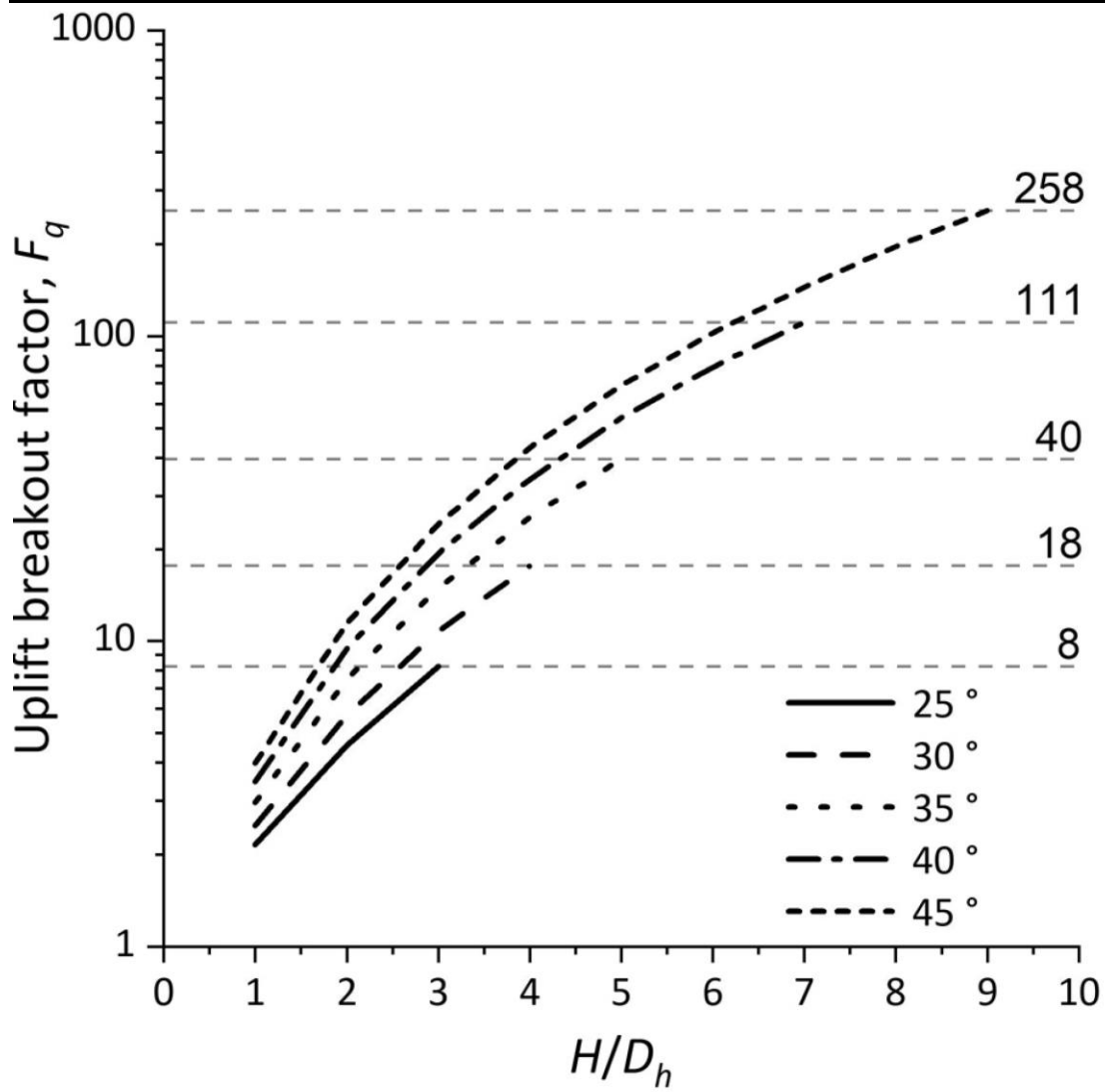


Figure 3

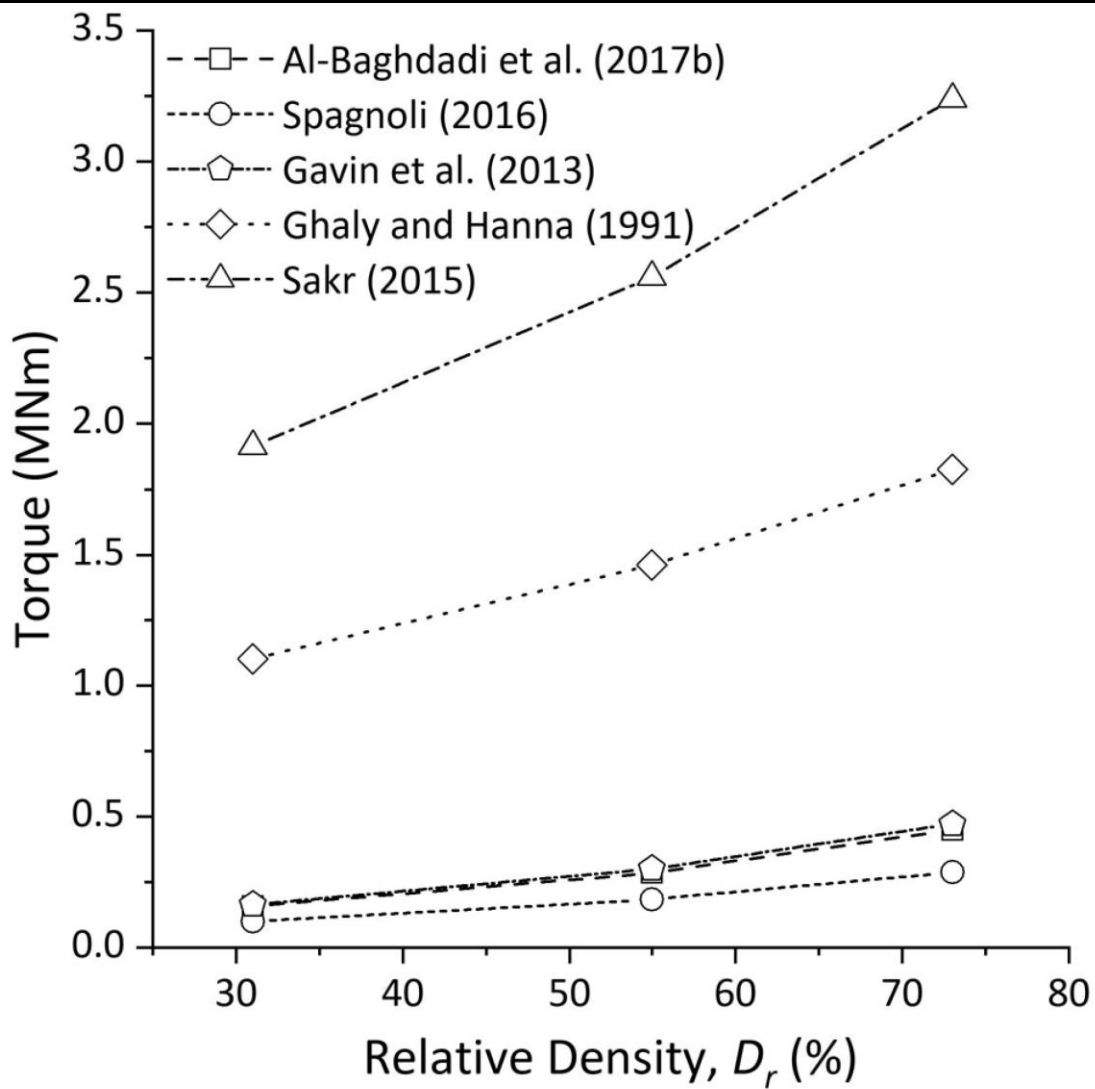


Figure 4

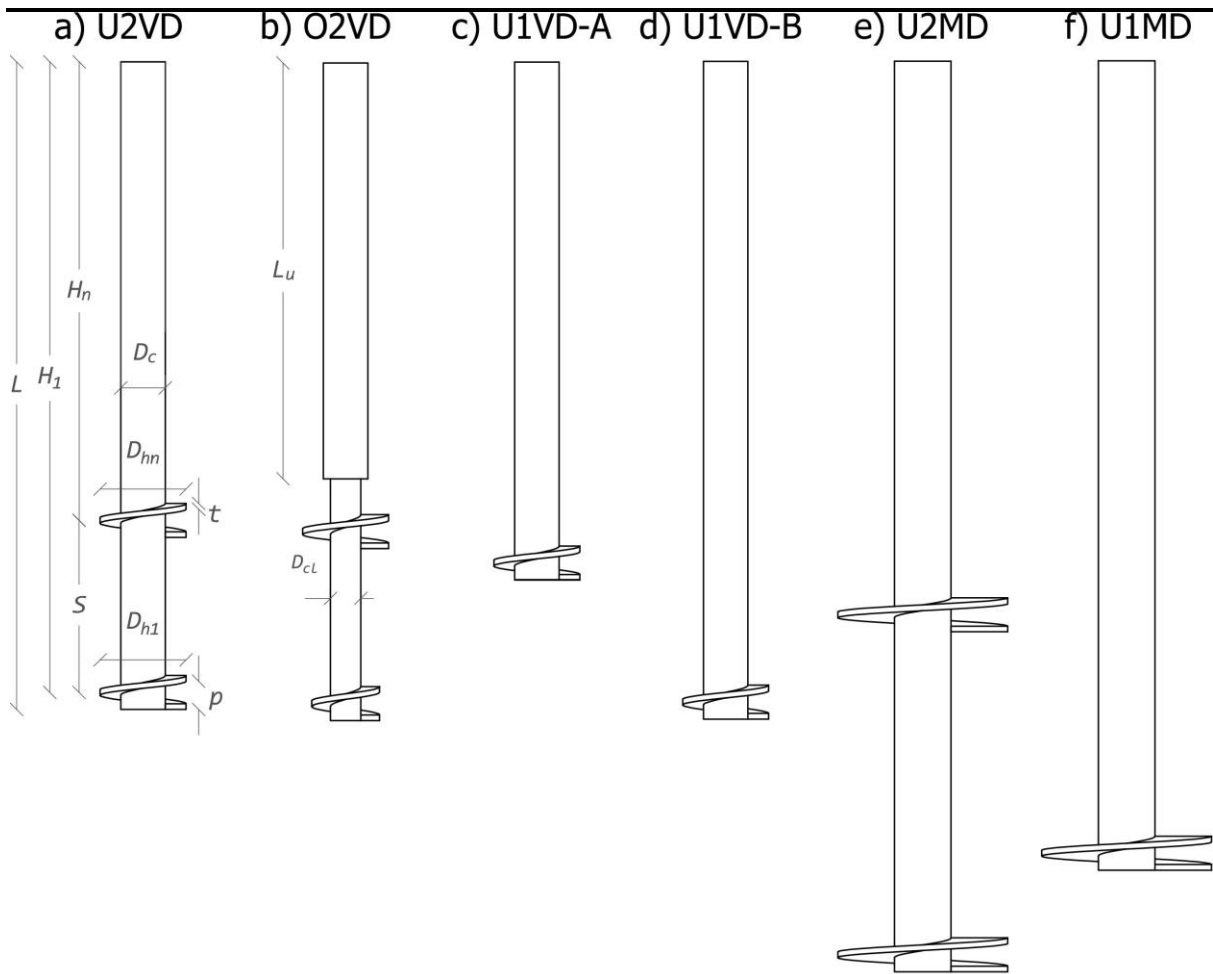


Figure 5

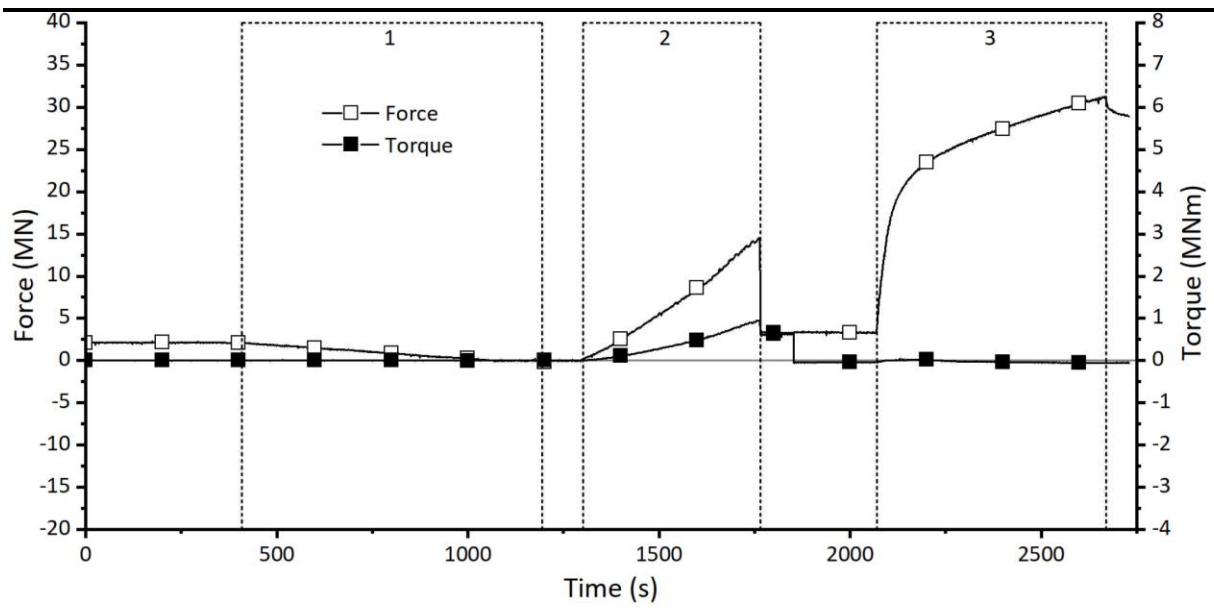


Figure 6a

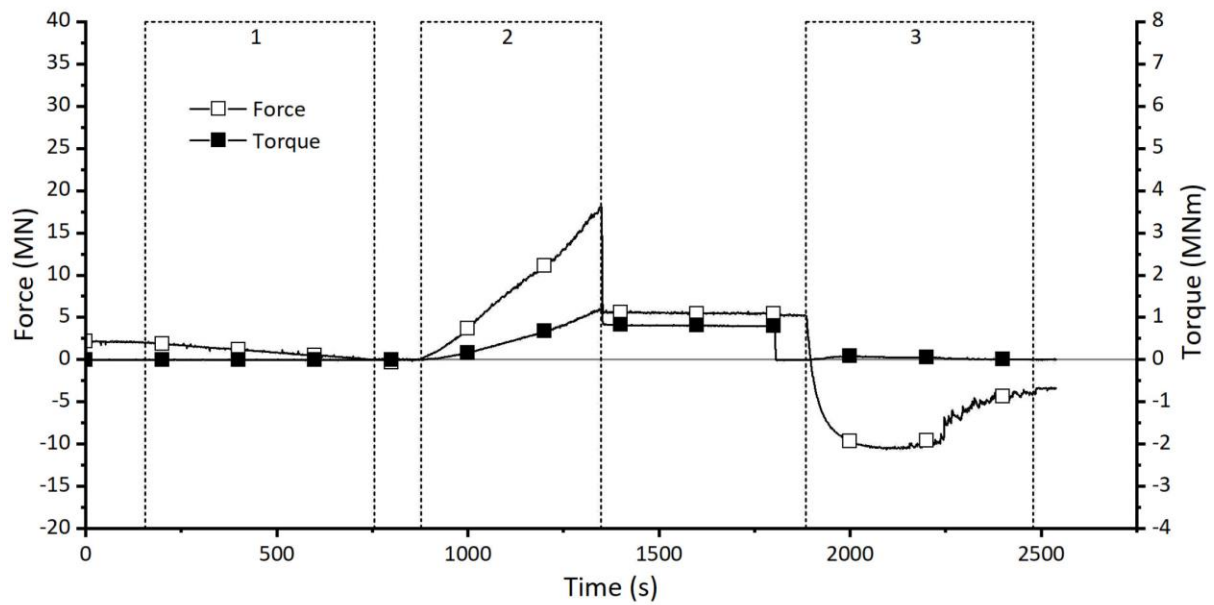


Figure 6

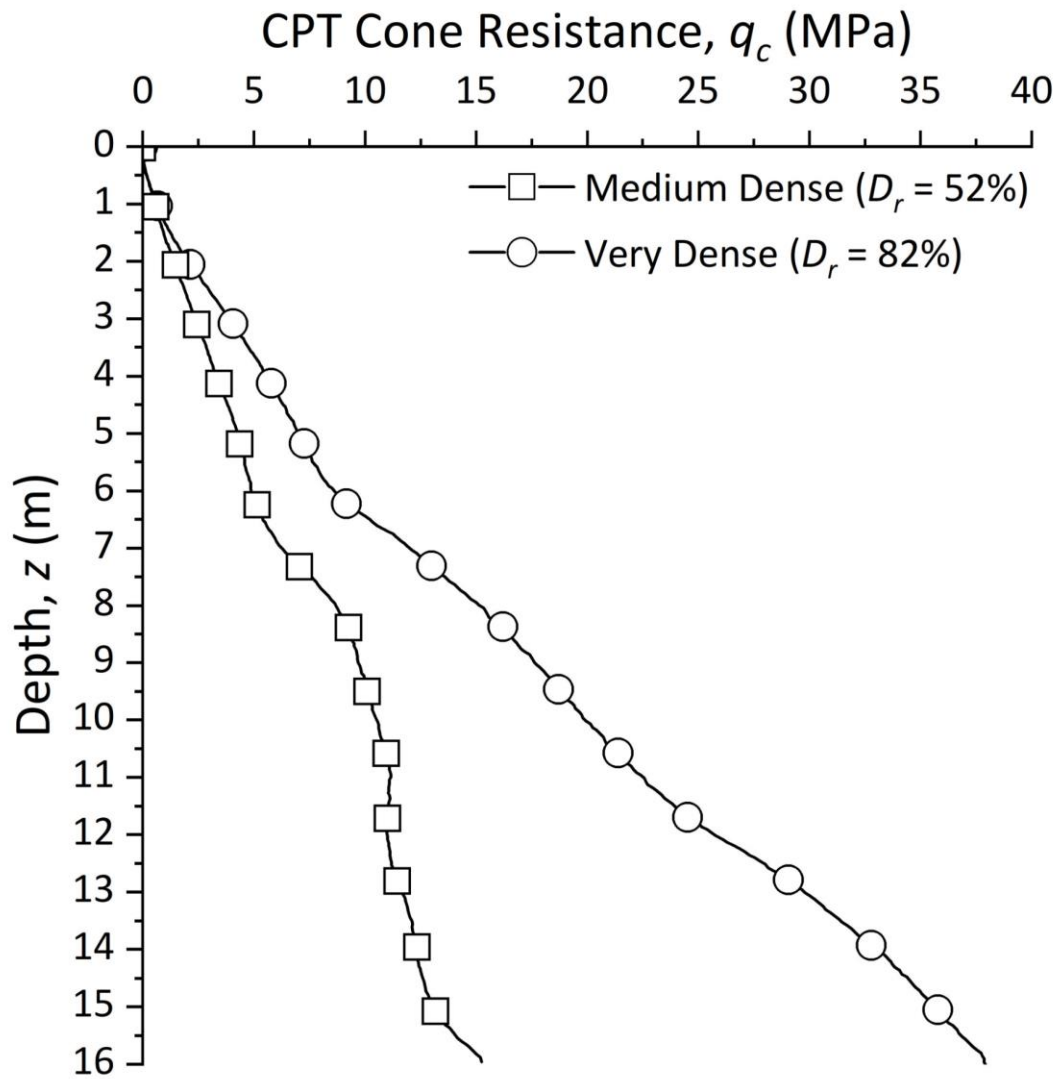


Figure 7

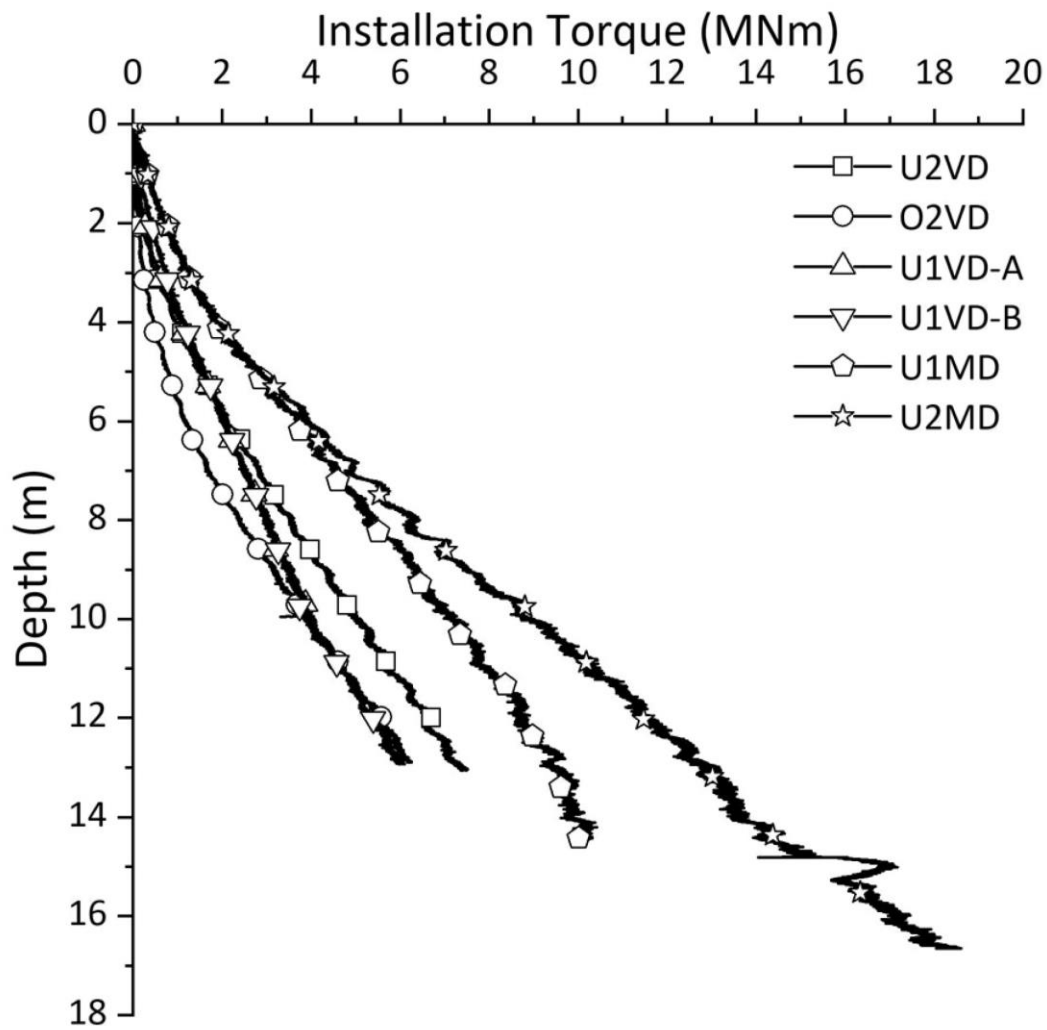


Figure 8

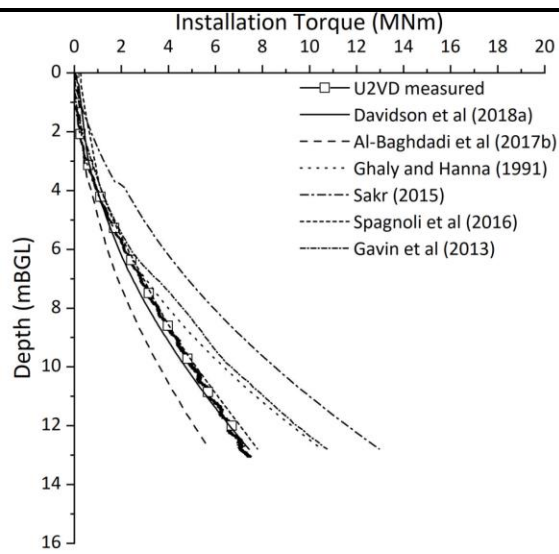


Figure 9a

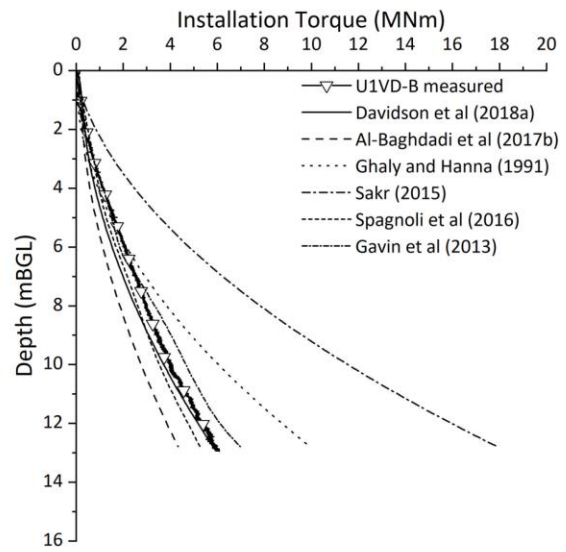


Figure 9b

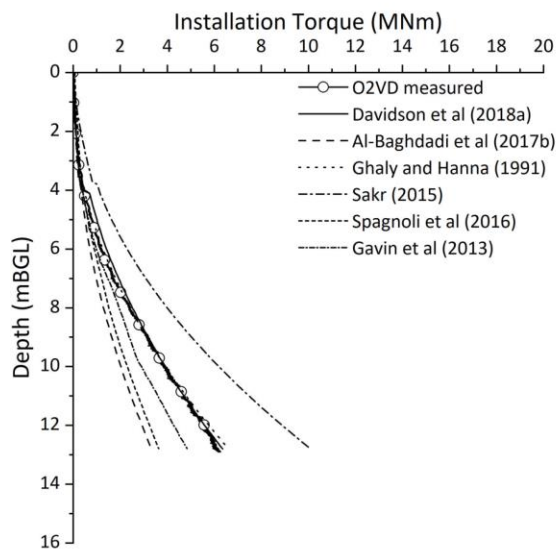


Figure 9c

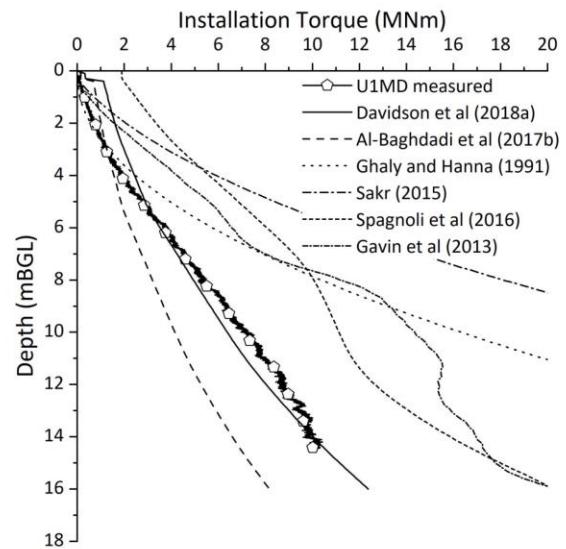


Figure 9d

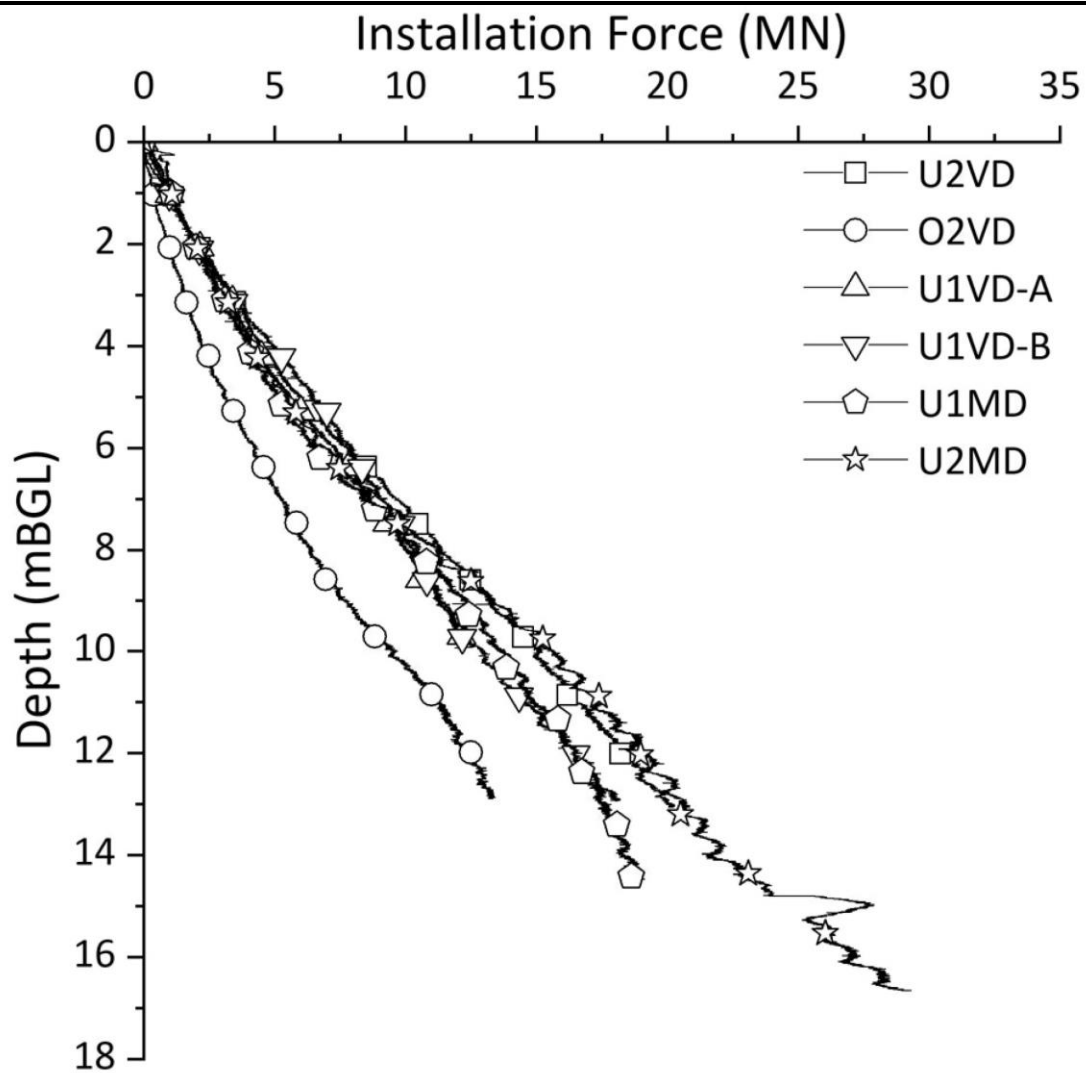


Figure 10

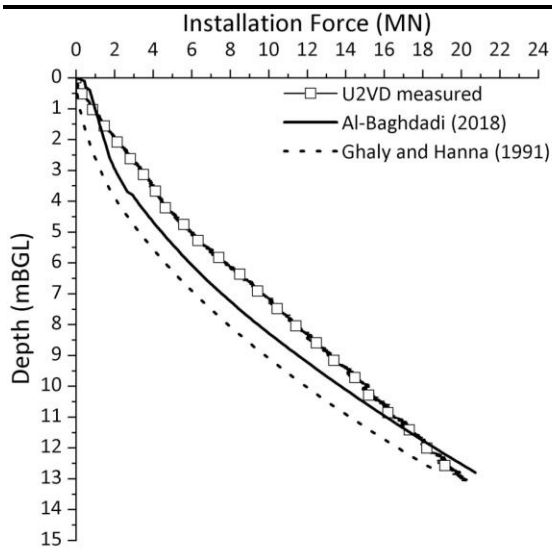


Figure 11a

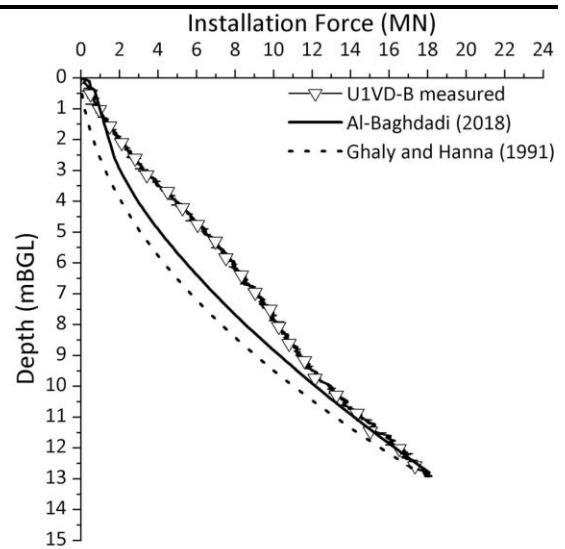


Figure 11b

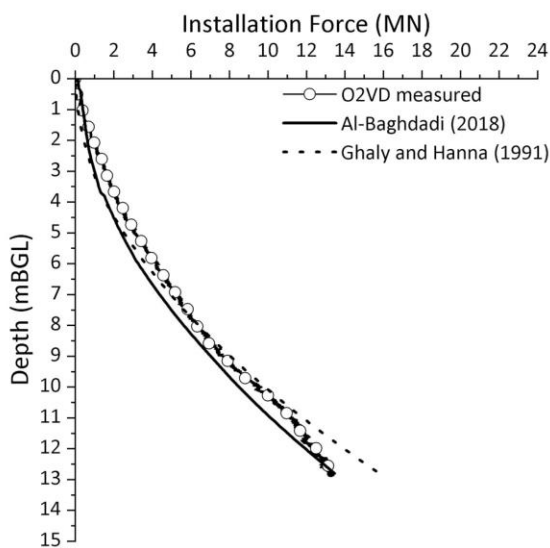


Figure 11c

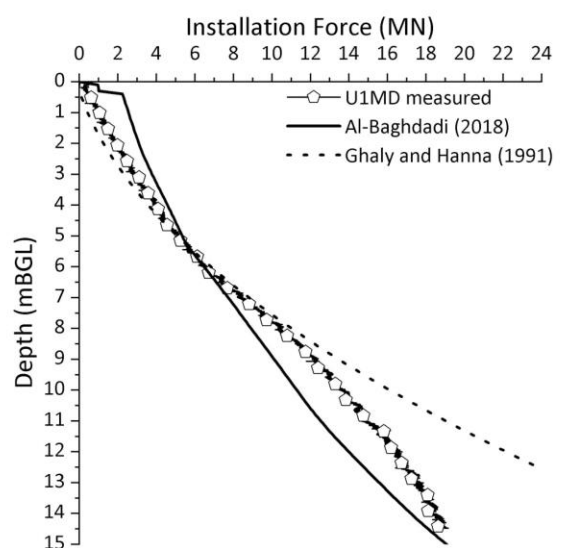


Figure 11d

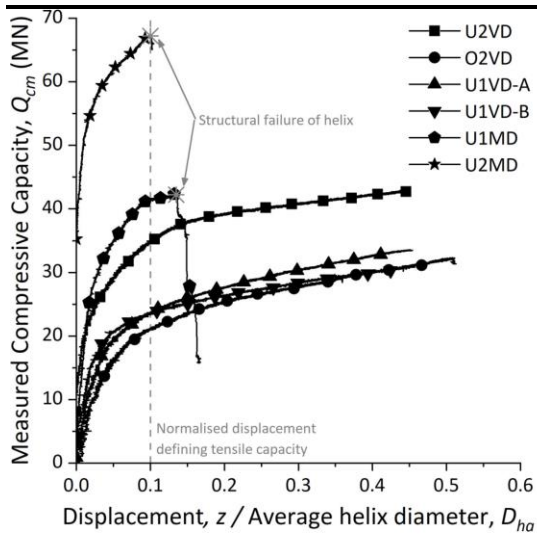


Figure 12a

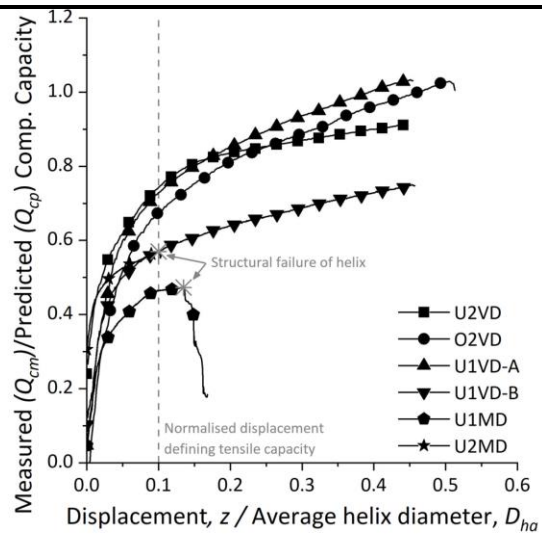


Figure 12b

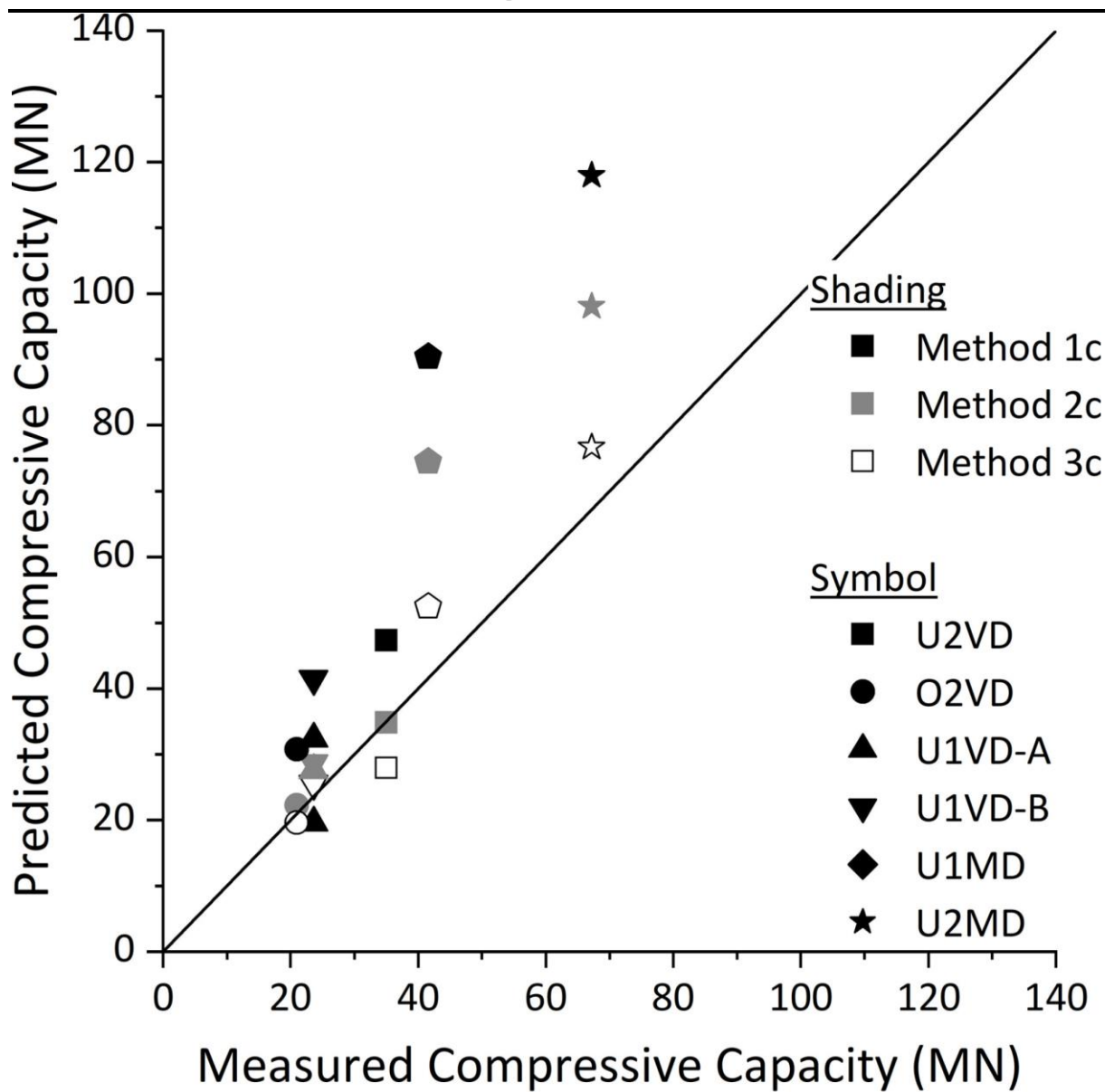


Figure 13

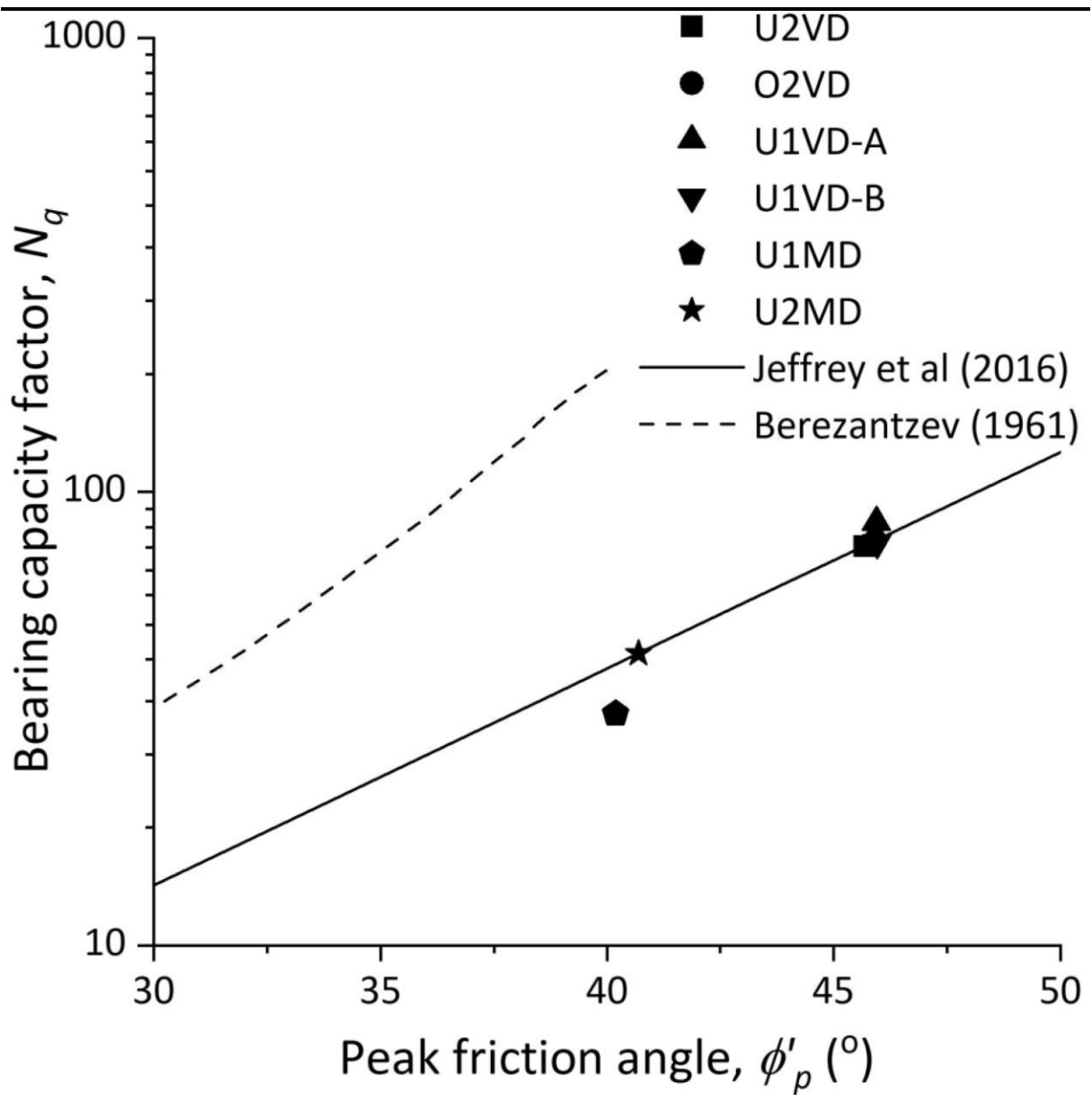


Figure 14

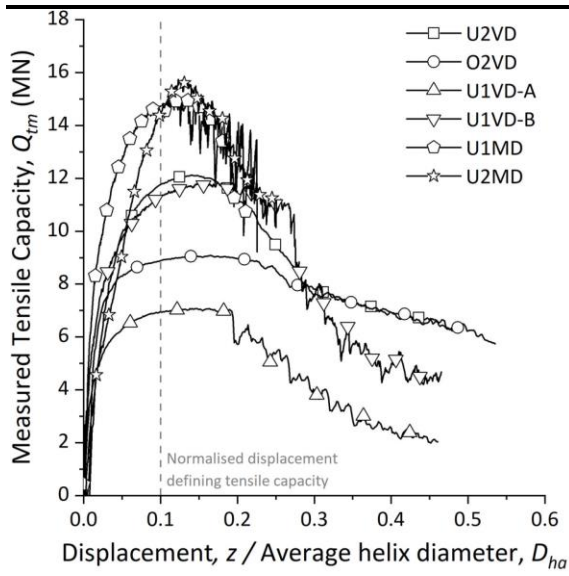


Figure 15a

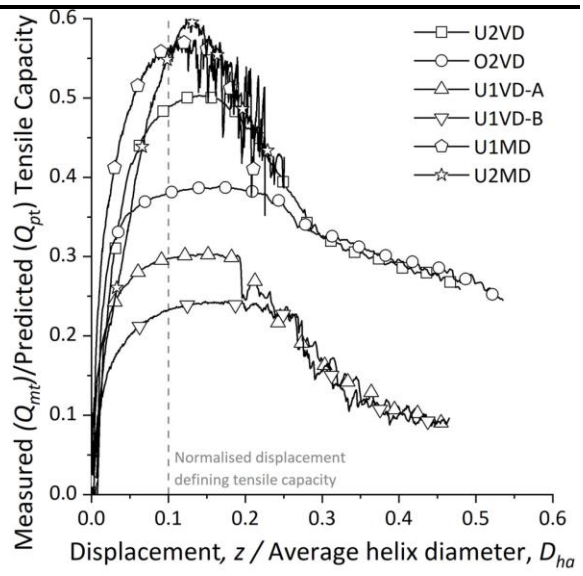


Figure 15b

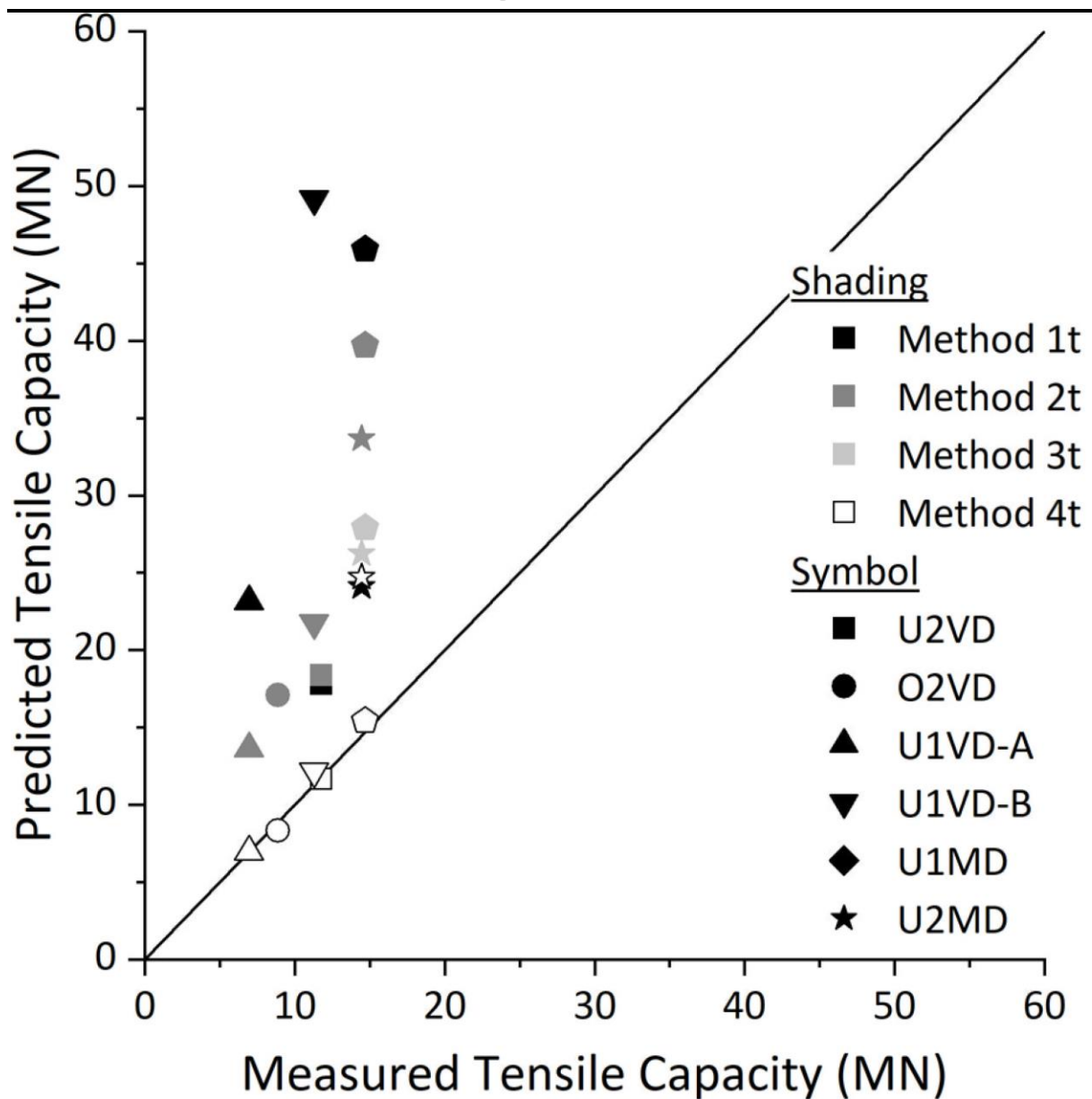


Figure 16